NASA TECHNICAL NOTE

NASA TN D-3164

NONADIABATIC PARTICLE LOSSES IN AXISYMMETRIC AND MULTIPOLAR MAGNETIC FIELDS

by J. Reece Roth

Lewis Research Center

Cleveland, Ohio

NATIONAL AERONAUTICS AND SPACE ADMINISTRATION - WASHINGTON, D. C. - DECEMBER 1965

NASA TN D-3164

NONADIABATIC PARTICLE LOSSES IN AXISYMMETRIC AND MULTIPOLAR MAGNETIC FIELDS

By J. Reece Roth

Lewis Research Center
Cleveland, Ohio

NATIONAL AERONAUTICS AND SPACE ADMINISTRATION

For sale by the Clearinghouse for Federal Scientific and Technical Information
Springfield, Virginia 22151 – Price $3.00

CONTENTS

NONADIABATIC PARTICLE LOSSES IN AXISYMMETRIC AND MULTIPOLAR MAGNETIC FIELDS

by J. Reece Roth

Lewis Research Center

SUMMARY

This report contains an analytical and experimental study of the nonadiabatic behavior of a single nonrelativistic charged particle in a magnetic field. Two magnetic field geometries were considered; an axisymmetric magnetic mirror, which was investigated by both analytical and experimental means, and a minimum-B configuration formed by the superposition of a multipolar (Ioffe) magnetic field on an axisymmetric magnetic mirror, which was studied only by analytical means. The nonlinear equations of motion for a charged particle in these magnetic field configurations were solved for 10^5 sets of initial conditions on a high-speed computer. A particle was considered to be nonadiabatic if its "adiabatic invariant" $M_4 \sim v_\perp^2/B$ varied by more than 5 percent during a single interaction with the magnetic mirror in question. By defining suitable dimensionless similarity parameters, it was found possible to summarize the computer results in a single analytical expression, which predicts the conditions under which nonadiabatic behavior will be observed. This similarity relation is a useful substitute for a closed-form solution to the nonlinear and nonholonomic mathematical problem, and may be used as a basis for correlating experimental data.

An experiment was devised to detect the enhanced particle losses resulting from nonadiabatic particle motion in an axisymmetric magnetic mirror. The results from a wide range of experimental conditions were plotted in terms of the similarity parameters found useful in correlating the analytical results and were found to obey the same similarity relation, but with different values of the constant parameters. This experimentally determined similarity relation gives the conditions for the onset of nonadiabatic losses in terms of the mirror ratio, particle energy, distance between mirrors, etc. This relation may be used as a design criterion to assure adiabatic confinement in axisymmetric magnetic mirrors of practical interest.

INTRODUCTION

Nature of Problem

One of the most promising methods of confining charged particles in a localized region of space is by trapping them between two "magnetic mirrors" - regions of increasing magnetic field strength. Particles that are confined in this general class of configurations are subject to several loss mechanisms that involve interactions among the particles, including microscopic and macroscopic plasma instabilities and collisional scattering. In this report, particle losses that result from the nonadiabatic interaction of a single charged particle with a magnetic mirror will be investigated. This report is motivated by the belief that nonadiabatic single particle losses should be understood well enough to be avoided, before one can usefully proceed to study collective loss processes.

It is helpful to distinguish three types of individual particle loss from magnetic mirrors: (1) adiabatic losses, which occur because the velocity vector of the particle lies within the escape cone in velocity space, (2) nonadiabatic losses which occur during a single interaction with a magnetic mirror, and are caused by an increase in the size of the loss cone above its adiabatic value, and (3) nonadiabatic losses resulting from a random-walk diffusion of the velocity vector into the escape cone after many reflections of the particle between magnetic mirrors.

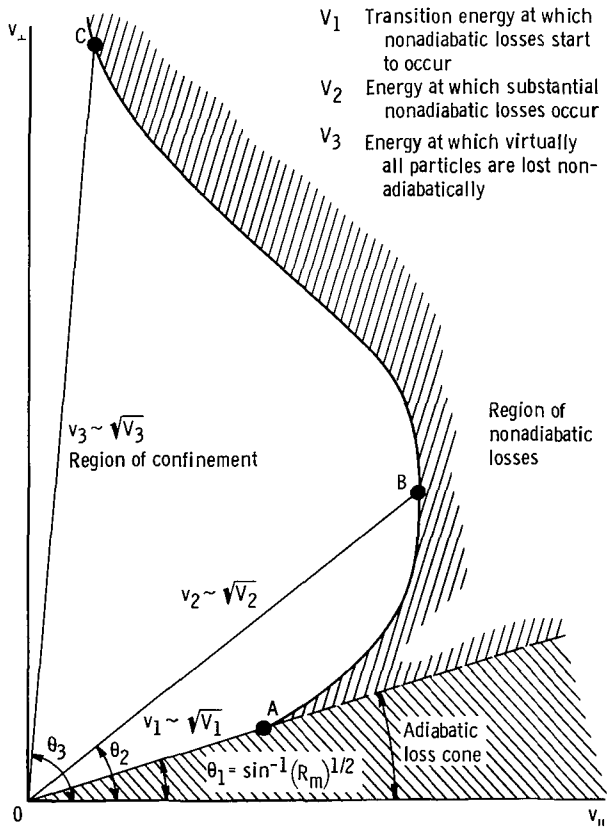

Figure 1. - Nonadiabatic loss regions in velocity space.

These loss mechanisms may be visualized by referring to figure 1, which represents a cross section of velocity space. $v_\parallel$ and $v_\perp$ are, respectively, the velocity components of the particle parallel and perpendicular to the local magnetic field line. (All symbols are defined in appendix A.) If the so-called "adiabatic invariant" (refs. 1 and 2)

$$M_4 = \frac{m^2}{e}\frac{v_\perp^2}{B} = \frac{m^2}{e}\frac{|\underline{v}\times\underline{B}|^2}{|\underline{B}|^3} \qquad (1)$$

is a constant of the motion, it can be shown that only those particles in the adiabatic

loss cone of figure 1 will escape through the magnetic mirror (see ref. 3). This loss cone has a half-angle in velocity space of

$$\theta_1 = \sin^{-1}\sqrt{R_m} \tag{2}$$

where $R_m = B_{min}/B_{max}$, and B_{min} and B_{max} are the minimum and maximum magnetic fields of the magnetic mirror. The adiabatic invariant M_4, however, is not a rigorous constant of the motion except when the ratio of the radius of gyration to the characteristic length of the magnetic field approaches zero. When this ratio is nonzero, as it is in all laboratory devices, M_4 is not constant, and the escape region in velocity space is larger than the adiabatic escape cone. This enlargement of the escape region has been documented in numerical computations by Garren, et al. (ref. 4).

Figure 1 is a schematic illustration of the regions of interest in velocity space. The regions of confinement and loss are separated by the boundary OABC, which is approximately a surface of rotational symmetry about the $v_{||}$ axis. The position of this boundary in figure 1 is schematic only. Adiabatic particle losses occur when the velocity vector of a particle lies in the adiabatic loss cone, where $\theta \leq \theta_1$. Single interaction nonadiabatic losses occur when the velocity vector of the particle lies in the escape region in the upper right of the figure. Multiple reflection nonadiabatic losses occur when the velocity vector of the particle diffuses across the boundary OABC into the loss region.

As will be discussed later, an initially isotropic distribution of particles in velocity space whose energy is below point A in figure 1 will suffer only adiabatic losses. A collection of particles whose energy corresponds to point B will suffer substantially more losses than is predicted by the adiabatic theory, since the effective escape cone angle is larger than that given by equation (2). At large energies corresponding to point C in figure 1, virtually all particles will be lost nonadiabatically. The experimental investigation described later in this report is concerned with determining the critical energy, corresponding to point A in figure 1, at which single interaction nonadiabatic losses begin to occur.

Relation of Nonadiabatic Effects to Economic and Stability Considerations

It will be shown that one of the similarity parameters appropriate to a discussion of nonadiabatic effects is ϵ, the ratio of the characteristic radius of gyration of the particle in question to z_o, the axial distance over which the magnetic field varies from B_{min} to B_{max}

$$\epsilon \equiv \frac{\langle R_\ell \rangle}{z_o} = \frac{mv}{eB_{av}z_o} \tag{3}$$

where v is the velocity based on the total energy of the particle in electron volts

$$v = \sqrt{\frac{2eV}{m}} \tag{4}$$

and B_{av} is the average magnetic field on the axis,

$$B_{av} = \frac{1}{2}(B_{min} + B_{max}) \tag{5}$$

Designing apparatus to confine particles by magnetic mirrors usually requires the mass and energy of the particles in question to be fixed by the objectives of the experiment. In consequence, the designer can adjust only the average magnetic field B_{av} or the apparatus dimensions z_o. In general, the capital costs of the apparatus will increase with the dimensions of the magnetic field z_o and with the average magnetic field strength B_{av}. These economic considerations will prompt the apparatus designer to make ϵ of a given apparatus as large as possible, since an adiabatic bottle with small ϵ is a much more costly container than an adiabatic bottle with large ϵ. If, however, ϵ is made too large, a magnetic bottle will suffer nonadiabatic losses, and not be fully effective in containing charged particles.

Stability considerations as well as economy play a role in determining the optimum value of ϵ. It has been shown by Kuo, et al. (ref. 5) that the stability of a plasma is enhanced if $\epsilon \geq 0.10$ (the so-called finite Larmor radius stabilization), and that this stabilizing effect is not present if $\epsilon \approx 0$, as the adiabatic theory requires. Finite radius of gyration stabilization therefore requires ϵ to be as large as possible. On the other hand, if ϵ is too large, the resulting nonadiabatic losses will enlarge the escape cone, and make the velocity distribution of the confined particles more anisotropic than it would otherwise be. Harris (ref. 6) has shown that anisotropies in velocity space promote the growth of instabilities. Therefore, ϵ should be made small enough to avoid nonadiabatic losses in order to reduce anisotropies in velocity space to an absolute minimum.

From the preceding discussion, it is evident that both economic and stability considerations dictate that ϵ should be as large as possible, without being so large that nonadiabatic losses occur. This critical value of ϵ is given, for a particular apparatus, by point A in figure 1, and it is the objective of the present report to determine this critical value of ϵ as a function of the relevant variables.

Previous Investigations

The equations of motion for a charged particle in a magnetic mirror are nonlinear, and, if the adiabatic invariant M_4 is constrained to vary by less than a specified amount, these nonlinear equations of motion are subject to a nonholonomic (inequality) constraint. The general mathematical problem has been studied by many investigators, nearly all of whom linearize the equations of motion by assuming that $\epsilon \ll 1$, or they treat ϵ as a small perturbation parameter. The conclusion of these investigations usually is that ϵ must be "small" if the particle motion is to be adiabatic and the reflection conditions predictable from the constancy of M_4. Many of these analytical investigations are discussed in a previous publication by the present author (refs. 1 and 2). The requirement that $\epsilon \ll 1$ for particles to be adiabatically confined is of limited value to the apparatus designer, because of its qualitative nature.

Only a few investigators have relaxed the requirement that ϵ be small and have attempted to predict the magnitude of the variation in M_4 for various magnetic field conditions. One such investigation was that of Grad and Van Norton (ref. 7), who have derived an expression for ΔM_4 in an idealized cusp geometry, and derived a loss probability from this expression, based on a random-walk diffusion of the velocity vector into the escape cone. Their results depend on the geometry of the magnetic field assumed as a starting point and do not appear to be relevant to the magnetic bottle configurations of interest in the present study.

Yoshikawa (ref. 8) derived an expression for ΔM_4 as a function of ϵ by a perturbation procedure and was able to show that ΔM_4 is proportional to ϵ^2 for small values of ϵ. The geometry he assumed was that of a magnetic mirror, and he observed the above proportionality when he integrated numerically the equations of motion for a few sets of initial conditions in the assumed magnetic field. Unfortunately, his results are not suitable for comparison with the present work, in which a single value of ΔM_4 was chosen as a basis for computation.

In addition to the work of Yoshikawa, computer studies of the exact nonlinear problem have been reported by Garren, et al. (ref. 4), and by the present author (refs. 1 and 2). The study by Garren, et al. covered approximately 100 sets of initial conditions and produced the important result that the escape cone for one or a few reflections of the particle is larger than that predicted in equation (2) by the adiabatic theory. Not enough sets of initial conditions were considered in the study by Garren, et al. to draw conclusions about the systematic trends of all the variables of interest in the problem. The previous computer study by the present author in references 1 and 2 covered 5×10^4 sets of initial conditions for a wide range of conditions in an axisymmetric magnetic mirror field. The results of this study had to be summarized in graphical form, but did give information about the systematic trends of the phenomena of interest.

Several experiments have been reported in which adiabatic confinement or nonadiabatic losses have been observed. These will be discussed subsequently.

Method of Approach

In this report, an extension of the method of similarity analysis is applied to the problem of determining under what conditions nonadiabatic losses will occur from an axisymmetric magnetic bottle and from a multipolar (Ioffe) field superimposed on an axisymmetric magnetic bottle. As understood in this report, similarity analysis consists of defining nondimensional variables that characterize the physical system under study and then finding analytical expressions, or "similarity relations", among these dimensionless variables that describe the behavior of the system. This similarity relation is, or should be, a quasi-solution to the equations of motion of the system. This method has been successful in describing diverse phenomena in the fields of aerodynamics and heat transfer, for example. In these fields the phenomena of interest are either too complex to be amenable to rigorous mathematical treatment, or they are described by nonlinear equations that do not admit of a rigorous and general solution. To provide some rational basis for correlating experimental data relating to nonadiabatic losses, an analogous, nonlinear, nonholonomic problem is solved on a high-speed computer. It is shown that the solution to this problem can be expressed in terms of similarity parameters related to one another by a similarity relation. The computer program used is given in appendix C by Paul Swigert.

An experimental technique was developed that is capable of detecting the conditions under which nonadiabatic losses begin to occur, analogous to point A in figure 1 (p. 2). These experiments were performed at various radii in an axisymmetric magnetic bottle. The experimental results were expressed in terms of the same similarity parameters found appropriate for the computer results, and the experimentally determined adiabatic-to-nonadiabatic transition boundary obeyed the same similarity relation as the computer results, although with somewhat different values of the constant parameters.

The present experimental results may be used as a criterion for the design of axisymmetric magnetic fields that will not suffer nonadiabatic particle losses. This criterion gives a compromise value of ϵ, which best satisfies the economic and stability constraints. By comparing the experimental results with the computer results (which hold for multipolar as well as axisymmetric magnetic mirrors), it is possible to lay down tentative design criteria for minimum-B magnetic fields that consist of a multipolar magnetic field superimposed on an axisymmetric magnetic field.

NUMERICAL ANALYSIS

Possible Approaches

This section describes an extensive series of numerical computations whose object was to simulate a common laboratory magnetic field geometry, and to map out the adiabatic-to-nonadiabatic transition region over a range of similarity parameters of practical interest.

In simulating particle confinement by magnetic mirrors on a computer, several alternatives suggest themselves: (1) A particle could be injected at the midplane and the equations of motion solved for a very large number of reflections, 10^6 for example, to see whether the particle is lost. (2) A single interaction with a magnetic barrier (a reflection or traversal) could be studied, and the boundary of the escape region in velocity space mapped out. (3) The fact that an increase in the escape cone angle is identified with a variation of M_4 could be used to terminate the computation when M_4 varies by more than a specified amount.

Practical difficulties forbid the first approach. Numerical errors, originating in the rounding-off of the numbers used in the numerical integration, introduce an error into the position and velocity of the particle, which becomes significant after at most a few reflections and which rapidly grows in magnitude. In the present series of computations, for example, these numerical round-off errors became significant after a single reflection of a particle, if $\epsilon \leq 0.01$. Single precision arithmetic was used. Even if rounding-off errors were not a problem, the time required to integrate numerically over 10^6 reflections would be prohibitive. On the average, the second approach required about 10 times as much computer time as the third, because if M_4 varied significantly, the total variation usually occurred early in the trajectory, before the particle either reflected from or passed through the magnetic barrier. In addition to this consideration, more particles had to be injected in velocity space to map out accurately the transition region if the second approach were used. A large total amount of computer time will be required in either case, and this total may be regarded as fixed. It is necessary to choose between either simulating the laboratory situation quite closely but with relatively few particles and over a rather limited range of variables, or using a less direct measure of particle confinement that enables one to use a large number of particles and cover a wide range of conditions.

The second approach was used by Garren, et al. (ref. 4), who were able to show that a significant variation of M_4 is identified with a significant opening-up of the escape cone in velocity space. The third approach was chosen in this investigation in order to cover as wide a range of conditions as possible. This choice transformed the problem of measuring nonadiabatic losses into the mathematical problem of solving a set of three coupled

nonlinear equations of motion, subject to the constraint that M_4 varies by less than some fixed amount over a single interaction of a particle with a magnetic barrier.

Setting up the Problem

A suitable magnetic field geometry must be chosen at the beginning of a numerical experiment of this nature. The geometry selected is a mathematically simple but nontrivial magnetic field, which is a good approximation to many axisymmetric and minimum-B laboratory devices. The basic axisymmetric magnetic field assumed is that used previously in references 1, 2, and 4. This magnetic field is generated by the current distribution

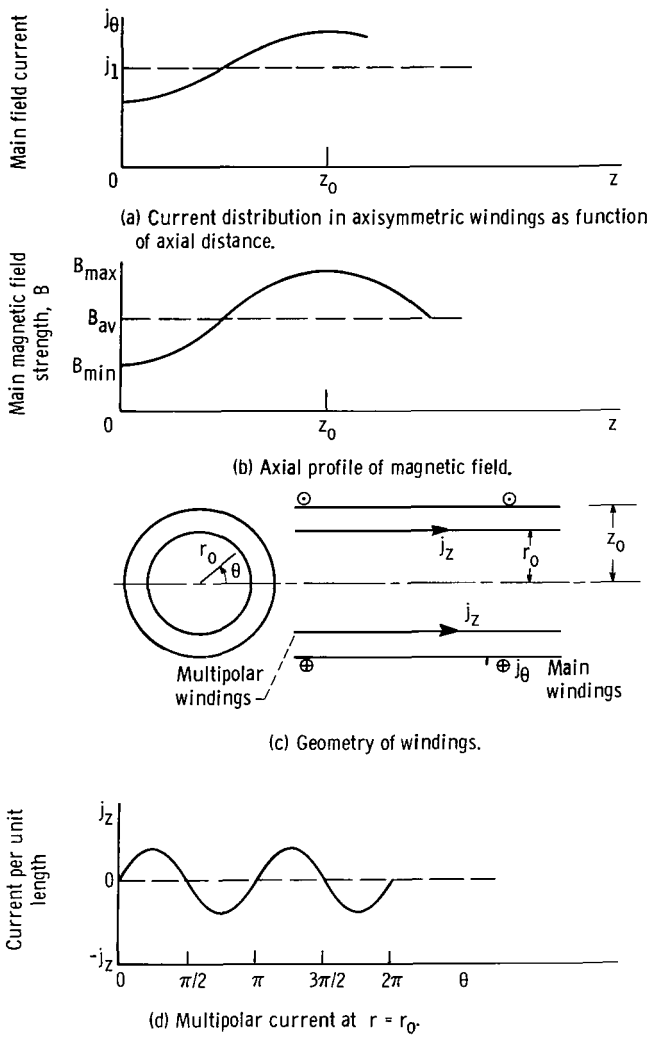

(a) Current distribution in axisymmetric windings as function of axial distance.

(b) Axial profile of magnetic field.

(c) Geometry of windings.

(d) Multipolar current at $r = r_0$.

Figure 2. - Magnetic field assumed in numerical computations.

$$j_\theta = j_1 + j_2 \cos \eta \tag{6}$$

flowing azimuthally in an infinitely long cylindrical current sheet. This configuration is illustrated in figure 2; η is the nondimensional axial coordinate, and is given by

$$\eta \equiv \frac{\pi z}{z_0} \tag{7}$$

where z_0 is the axial distance between the points of minimum and maximum current. It has been assumed that the radius of this current sheet is equal to z_0. The vector potential inside the current sheet is (refs. 1 and 2)

$$A_\theta = \mu_0 j_2 z_0 K_1(\pi)[\alpha C_1 + I_1(\alpha)\cos \eta] \tag{8}$$

where I_0, I_1, and K_1 are the Bessel functions of imaginary argument, and the constant C_1 is given by

$$C_1 = \frac{I_0(\bar{\alpha})}{2} \frac{(R_c + 1)}{(R_c - 1)} = \frac{B_{av}}{2\mu_0 j_2 \pi K_1(\pi)} \tag{9}$$

where α is the nondimensional radius,

$$\alpha \equiv \frac{\pi r}{z_o} \tag{10}$$

and R_c is the mirror ratio at the radius $\overline{\alpha}$, the radius of the particle when $B = B_{min}$:

$$R_c \equiv \frac{B_{min}(\overline{\alpha})}{B_{max}(\overline{\alpha})} = \frac{B(\alpha = \overline{\alpha}, \eta = 0)}{B(\alpha = \overline{\alpha}, \eta = \pi)} \tag{11}$$

The mirror ratio defined in equation (11) varies between zero and unity, contrary to some definitions that define it as the inverse of equation (11) and/or in terms of the magnetic field on the axis. The vector potential of equation (8) generates an infinite series of magnetic bottles each of which, for $\alpha \leq 0.75$, is a good approximation to the magnetic bottles generated in laboratory apparatus.

Since minimum-B as well as axisymmetric geometries are to be studied, a multipolar field must be added to equation (8). The assumed multipolar field is generated by n pairs of infinitely long currents located on an infinitely thin cylindrical current sheet of radius r_o. This current is assumed to be spread out in azimuthal angle, as shown in figure 2, and to flow in the η-direction. The assumed sinusoidal variation of current with azimuthal angle is intended to approximate spread-out multipolar conductors encountered in practice. The vector potential of the multipolar field is then equal to

$$A_z = \frac{B_m r_o}{n} \left(\frac{\alpha}{\alpha_o}\right)^n \sin n\theta \tag{12}$$

where B_m is the magnetic field intensity at the multipolar current sheet due to the multipolar field alone, and α_o is the nondimensional radius at which the multipolar current sheet is located.

The total vector potential of the assumed magnetic field is then

$$\underline{A} = \mu_o j_2 z_o K_1(\pi)[\alpha C_1 + I_1(\alpha) \cos \eta]\underline{i}_\theta + \frac{B_m r_o}{n}\left(\frac{\alpha}{\alpha_o}\right)^n \sin n\theta \, \underline{i}_z \tag{13}$$

The Lagrangian for a single, positive, nonrelativistic charged particle is

$$L = \frac{1}{2} m(\dot{r}^2 + r^2\dot{\theta}^2 + \dot{z}^2) + e(\underline{A} \cdot \underline{v}) \tag{14}$$

If the time is nondimensionalized with respect to ω_{av}, the frequency of gyration based on B_{av}, the nondimensional time is given by

$$\tau = \omega_{av} t \equiv \frac{eB_{av}t}{m} \tag{15}$$

where B_{av} is the average magnetic field on the axis, defined by equation (5). If the derivative with respect to nondimensional time τ is denoted by $'$, that is, $d\alpha/d\tau = \alpha'$, the Lagrangian may be written in the form

$$L = \frac{e^2 B_{av}^2 z_o^2}{m\pi^2}\left[\frac{1}{2}(\alpha'^2 + \alpha^2\theta'^2 + \eta'^2 + \alpha^2\theta') + \frac{1}{2C_1}\alpha\theta' I_1(\alpha)\cos\eta + \frac{B_m}{nB_{av}}\frac{\alpha^n}{\alpha_o^{n-1}}\eta'\sin n\theta\right] \tag{16}$$

In terms of a nondimensional generalized coordinate χ, the Lagrangian equations are

$$\frac{d}{dt}\left(\frac{\partial L}{\partial \chi'}\right) - \frac{\partial L}{\partial \chi} = 0 \tag{17}$$

The dimensionless equations of motion are then

$$\alpha'' - \alpha\theta'^2 - \alpha\theta' - C_2\alpha\theta' I_o(\alpha)\cos\eta - C_3\eta'\alpha^{n-1}\sin n\theta = 0 \tag{18}$$

$$\alpha\theta'' + 2\theta'\alpha' + \alpha' - C_2\eta' I_1(\alpha)\sin\eta + C_2\alpha' I_o(\alpha)\cos\eta - C_3\eta'\alpha^{n-1}\cos n\theta = 0 \tag{19}$$

$$\eta'' + C_3\alpha'\alpha^{n-1}\sin n\theta + C_3\theta'\alpha^n\cos n\theta + C_2\alpha\theta' I_1(\alpha)\sin\eta = 0 \tag{20}$$

The constant C_2 that appears in equations (18) to (20) is related to the magnitude of the variation of the main axisymmetric magnetic field and is equal to

$$C_2 \equiv \frac{1}{2C_1} = -\frac{(1 - R_c)}{I_o(\bar{\alpha})(1 + R_c)} \tag{21}$$

The constant C_3 is related to the magnitude of the multipolar magnetic field, to the number of pairs of conductors, and to the radial position of the multipolar current sheet:

$$C_3 \equiv \frac{B_m}{B_{av}\alpha_o^{n-1}} = \frac{2R_m\delta}{\pi^{n-1}(1 + R_m)} \tag{22}$$

where R_m is the mirror ratio on the axis,

$$R_m \equiv \frac{B(\alpha = 0, \eta = 0)}{B(\alpha = 0, \eta = \pi)} \tag{23}$$

and δ is given by

$$\delta \equiv \frac{B_m z_o^{n-1}}{B_{min} r_o^{n-1}} \tag{24}$$

The preceding equations of motion (eqs. (18) to (20)) are intrinsically nonlinear. If the field-defining constants C_2 and C_3 were set equal to zero, the motion would be that of a particle moving in the uniform magnetic field of an infinite solenoid. A perturbation approach is not indicated, since it would necessarily restrict C_2 and C_3 to small values and exclude those large variations in the magnetic fields that are most effective in confining charged particles. Without a general closed-form solution to these nonlinear equations, the future position and velocity of a particle cannot be predicted from a knowledge of its present position and velocity without numerically integrating the equations of motion. There is no simple way to tell whether a given particle will be reflected or not, and the adiabatic invariant M_4 is often used in lieu of a closed-form solution to the problem to provide this information. The only feasible way of studying the nonadiabatic variations of M_4 is to solve equations (18) to (20) on a computer by numerical integration, pending the unlikely event of a nontrivial, closed-form, general solution of these equations.

Method of Computation

A particle was considered to be nonadiabatic in these numerical computations if ΔM_4 was greater than 5 percent while the particle was moving in the volume of space defined by $0 \leq \eta \leq \pi$ and $0 \leq \alpha \leq \pi$. The 5-percent criterion was chosen because this degree of variation occurred for the same values of ϵ and R_c where early experiments showed the adiabatic-to-nonadiabatic transition to occur (refs. 1 and 2).

In the numerical computations, a particle was injected in the direction of positive η

at the midplane $\eta = 0$, and its motion followed until it was reflected, until it escaped through the magnetic mirror at $\eta = \pi$, or until it became nonadiabatic. The positions and velocities corresponding to each trajectory point from the computer solution were used to calculate the kinetic energy

$$T = \dot{\alpha}'^2 + \alpha^2\dot{\theta}'^2 + \dot{\eta}'^2 = \pi^2\epsilon^2 \tag{25}$$

and the adiabatic invariant M_4 at each trajectory point. The constancy of the kinetic energy was used as a check on the round-off errors in the computation. If T varied by more than five parts in 10^5 from one trajectory point to another, the new point was rejected, and the integration interval halved until the variation of T was below that limit. In no case was the cumulative error as large as a 1-percent drift in T from the initial to the final trajectory point.

The value of M_4 was calculated at each trajectory point, and if this was either higher or lower than all previous values, the previous extreme value was replaced with the new extreme value. When the ratio of the extreme values of M_4 was

$$\Delta M_4 = \left| \frac{M_{4,\,high} - M_{4,\,low}}{M_{4,\,low}} \right| \geq 0.05 \tag{26}$$

the particle was considered to be nonadiabatic, and the computation of that particular particle terminated.

As equations (18) to (20) are written, nine initial conditions are required for the problem. These are α, θ, η, $\dot{\alpha}$, $\dot{\theta}$, $\dot{\eta}$, C_2, C_3, and n. It would require a prohibitive amount of computer time to map out the adiabatic-to-nonadiabatic transition surface in this nine-dimensional space, so that the required number of initial conditions were reduced. The initial condition $\eta = 0$ was used in all cases, thereby defining adiabaticity in terms of a single interaction with a magnetic mirror. The three velocity initial conditions were replaced by two variables, ϵ and F, where the relation of ϵ to the velocity components is given by equation (25). The symbol F represents the fraction of particles distributed over a hemisphere in velocity space that is adiabatic for given values of α, θ, η, C_2, C_3, and n. In the present computation, the 20 particles listed in table I were used to determine F. These 20 points gave essentially the same results as the 85 more evenly distributed points used previously in references 1 and 2.

As will be discussed subsequently, a preliminary set of computations showed that a particle was most apt to be nonadiabatic if it were injected at $\theta = 0$, the position between Ioffe bars. For this reason, and to conserve computer time, the azimuthal angle θ was set equal to zero for all cases. It was deemed desirable to replace the parameters C_2

and C_3 with more familiar parameters, whose physical significance is more easily grasped R_c, R_m, and δ. The relation among these constants is given by equations (21) and (22). The computer program is expressed in terms of the parameters α, ϵ, F, R_c, δ, and n. The computer program is discussed in appendix C.

Correlating Results of Numerical Computations

In the numerical computations, the variables α, ϵ, R_c, δ, and n were treated as independent, with F, the fraction of particles adiabatic, as the dependent variable to be calculated by following the 20 trajectories whose initial conditions are listed in table I. The nondimensional radius α was assigned eight values over the range $0.05 \leq \alpha \leq 2.50$, the adiabatic parameter ϵ assumed six values over the range $0.01 \leq \epsilon \leq 0.06$; the parameter R_c took on six to twelve values over the range $0.1 \leq R_c \leq 1.00$; the parameter δ assumed six values over the range $0 \leq \delta \leq 1.50$; and the parameter n took on two values, $n = 2$ (quadrupole configuration), and $n = 3$ (hexapole configuration). This amounts to about 5×10^3 cases, or, since there are 20 trajectories per case, 10^5 individual particle trajectories. A limited number of computations were made for $n > 3$ and $\theta \neq 0$ to assess the influence of these variables.

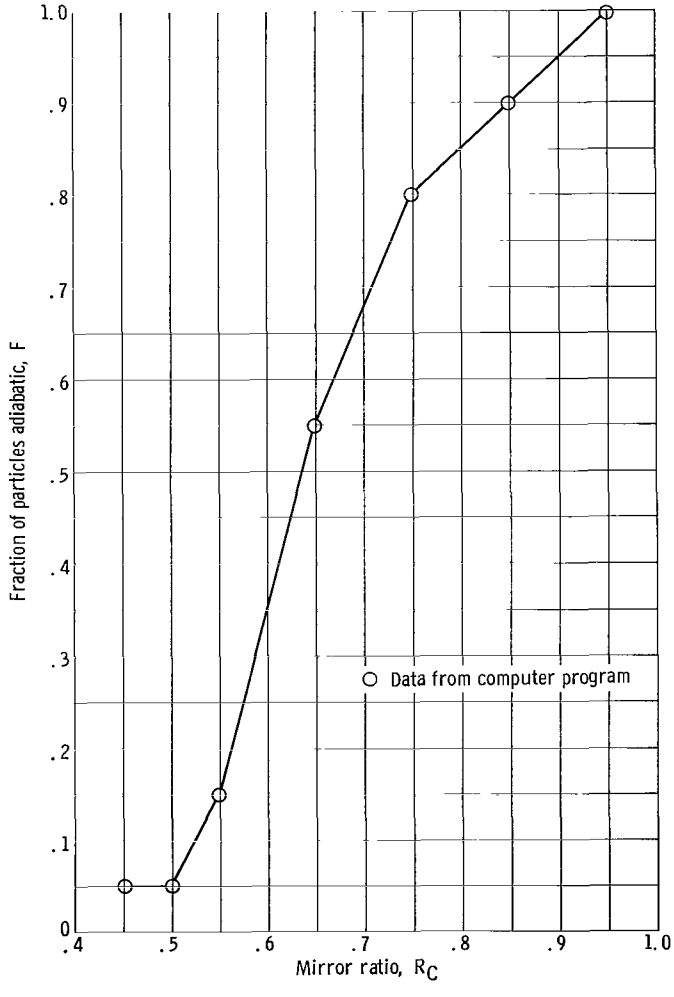

Figure 3. - Fraction of particles adiabatic as function of mirror ratio. Radial mirror ratio, δ, 0.25; multipolar currents, n, 2; nondimensional radius, α, 1.50; adiabatic parameter, ϵ, 0.02.

Clearly, such a mass of data cannot be properly interpreted without some means of correlating it, so that the relative importance of the variables and their systematic relation to one another is evident. The dimensionless variables listed in the preceding paragraph are a set of similarity parameters for the problem. The correlation procedure consists of cross-plotting the similarity parameters, and finding an analytical expression that best fits the cross plot. A sample series of

similarity plots will be discussed to illustrate the method of correlating the data, and also to illustrate the generally excellent fit of the data to the similarity relations. Figure 3 shows a plot of F, the fraction of particles adiabatic, as a function of the mirror ratio R_c, for the particular values $\delta = 0.25$, $n = 2$, $\alpha = 1.50$, and $\epsilon = 0.02$. The seven data points represent seven different computer runs, each of which used the 20 sets of initial conditions listed in table I.

The value of R_c corresponding to values of F of 0.1, 0.5, and 0.9 adiabatic was read from figure 3 and is plotted in figure 4, which also contains data from five other plots similar to figure 3, over the range $0.01 \leq \epsilon \leq 0.06$. The data for a given percentage adiabatic lie along a straight line, which implies a similarity relation of the form

$$R_c = \left(\frac{\epsilon}{\epsilon_0}\right)^A \tag{27}$$

In order to improve the objectivity and precision of the curve fitting of this data, a computer program was devised that fitted a least-squares straight line to the logarithms of ϵ and R_c. Figure 4 illustrates the particular values $n = 2$, $\delta = 0.25$, and $\alpha = 1.50$. The similarity relation of equation (27) held for all values of n, δ, and α investigated, and failed only for ϵ greater than 0.08. In the latter case, the data fell below the curve given by equation (27) and became asymptotic to the line $R_c = 1$.

The parameter ϵ_0 is shown in figure 5 plotted as a function of F, the fraction of particles adiabatic, for two particle radii, $\alpha = 0.50$ and 1.50. These curves can be approximated by the sum of two power-law terms:

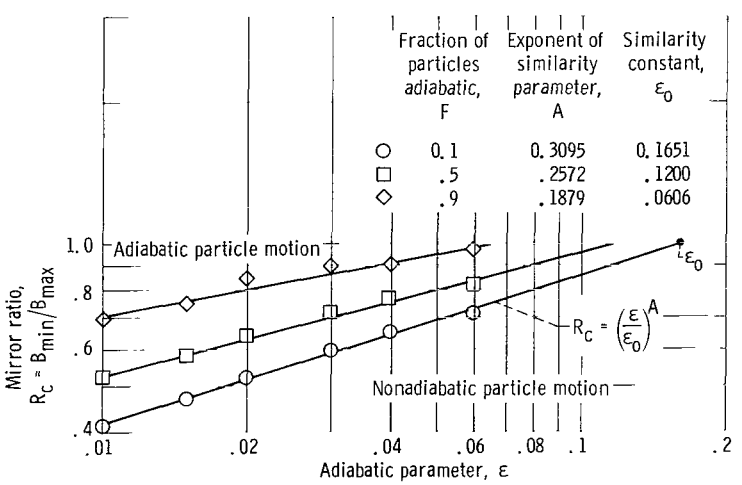

Figure 4. - Mirror ratio R_c as function of adiabatic parameter ϵ. Radial mirror ratio, δ, 0.25; multipolar currents, n, 2; nondimensional radius, α, 1.50.

$$\epsilon_o = C_4(1 - F)^{E_1} + C_5(1 - F)^{E_2} \tag{28}$$

A computer program was devised to fit all the values of ϵ_o for given values of n, α, and δ to this relation. The fit of the data to the expression in equation (28) was good in all cases investigated. It was not possible to correlate the parameters C_4, C_5, E_1, and E_2 as a function of n, δ, or α; they are given in tabular form in table II.

The exponent A of the similarity relation of equation (27) is plotted in figure 6 as a function of the nondimensional radius α, for the particular case $\delta = 0.25$, $F = 0.1$, and $n = 2$. A straight line was fitted to the data with the same computer program used for the original similarity relation. The exponent A is of the form

$$A = A_o \alpha^K \tag{29}$$

where both A_o and K are functions of δ, n, and F. The scatter of the points in figure 6 is among the worst of all the data.

It was possible to correlate the parameter A_o by plotting it as a function of 1 - F, the fraction of particles which are nonadiabatic. The values of A_o for $\delta = 0.25$ and $n = 2$ are shown in figure 7. Evidently, A_o obeys a similarity relation of the form

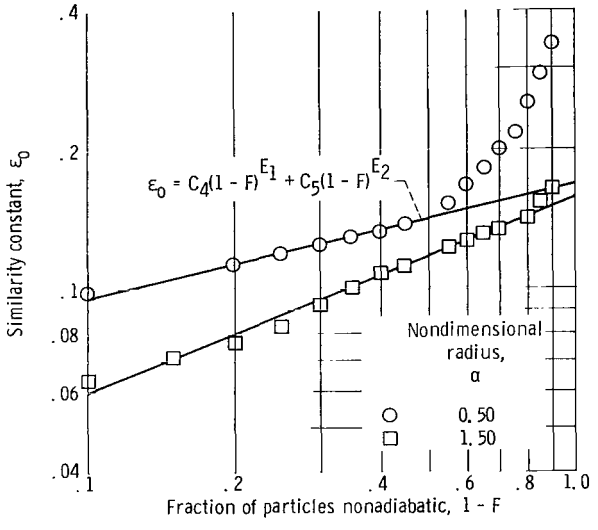

Figure 5. - Similarity constant ϵ_o as function of fraction of particles nonadiabatic 1 - F. Radial mirror ratio, δ, 0.25; multipolar currents, n, 2.

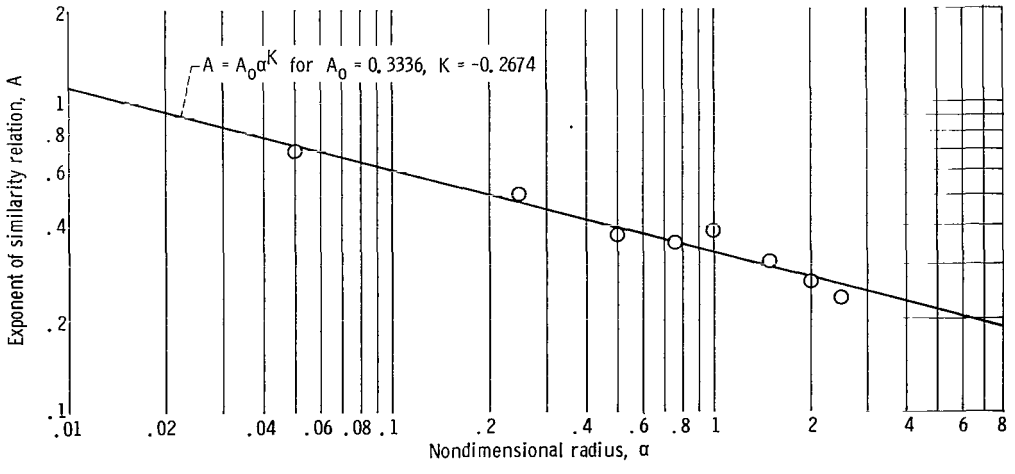

Figure 6. - Exponent A as function of nondimensional radius α. Radial mirror ratio, δ, 0.25; multipolar currents, n, 2; fraction of particles adiabatic, F, 0.1.

$$A_o = A_{oA}(1 - F)^{C_6} \tag{30}$$

Equation (30) held true for the entire range of δ and n studied.

The exponent K was also plotted as a function of 1 - F, as shown in figure 8. The exponent K is of the form

$$K = K_o(1 - F)^{C_7} \tag{31}$$

where K_o and C_7 are functions only of n and δ. The similarity relation in equation (31) held for the other values of n and δ investigated.

If equations (29) to (31) are combined, it can be seen that the exponent in equation (27) may be written

$$A = A_{oA}(1 - F)^{C_6} \alpha^{K_o(1-F)^{C_7}} \tag{32}$$

where the parameters A_{oA}, C_6, K_o, and C_7 are functions only of n and δ. It was not possible to correlate these parameters further; they are listed in table III for the values of n and δ studied.

If equations (27), (28), and (32) are combined, the master similarity relation that describes the results of the computation can be formed:

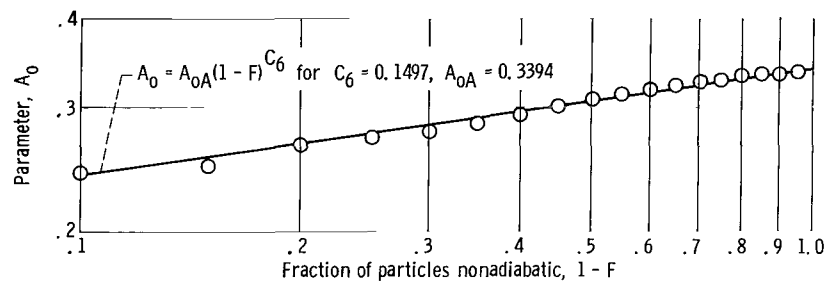

Figure 7. - Parameter A_o as function of fraction of particles nonadiabatic 1 - F. Radial mirror ratio, δ, 0.25; multipolar currents, n, 2.

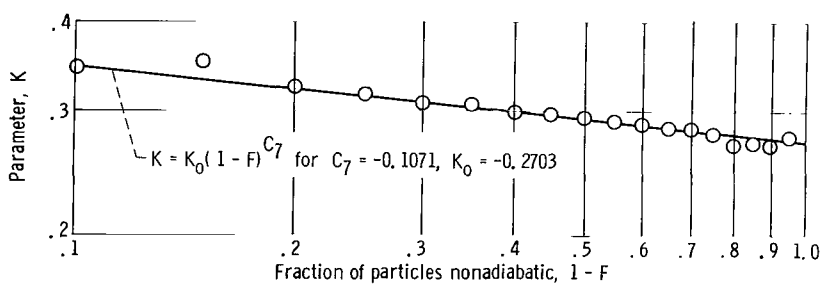

Figure 8. - Parameter K as function of fraction of particles nonadiabatic 1 - F. Radial mirror ratio, δ, 0.25; multipolar currents, n, 2.

$$R_c = \left[\frac{\epsilon}{C_4(1 - F)^{E_1} + C_5(1 - F)^{E_2}} \right]^{A_{oA}(1-F)^{C_6} \alpha^{K_o(1-F)^{C_7}}} \tag{33}$$

Equation (33) is the desired similarity relation that, together with the values of the constants listed in tables II and III, summarizes the behavior of the approximately 10^5 particles that were studied. Equation (33) may be thought of as a particular solution to the original nonlinear and nonholonomic mathematical problem. It is, perhaps, worth noting that the usual perturbation approach (which consists of linearizing the original equations of motion and then trying to derive an expression like eq. (33) from the linearized equation) has been inverted. Instead, a large number of exact solutions to the problem have been amassed, and equation (33) has been derived from them.

There is a fundamental difficulty with the conventional perturbation methods that is absent - or at least not as severe - in the procedure used here. It is never possible to be sure that the solution to an approximate, linearized problem bears any relation to the solution of the exact, nonlinear problem. The procedure used here makes it possible to test how well equation (33) agrees with the exact solutions from which it was derived. The agreement of the exact solutions with the value calculated from equation (33) was measured by the quantity

$$\Delta \equiv \frac{R_{c,e} - R_c}{R_{c,e}} \tag{34}$$

where R_c is the value calculated by substituting the appropriate value of ϵ and the corresponding parameters from tables II and III into equation (33), and $R_{c,e}$ is the mirror ratio from the exact computation, as taken from the raw data charts such as figure 3. The number of cases in each interval of Δ is shown in figure 9.

The distribution of error in figure 9 is roughly Gaussian, with a standard deviation of ±6 percent. It is not possible, in the present investigation, to distinguish between errors caused by interpolating between the computer-derived data points on the raw data plots, similar to figure 3, and errors that come about because equation (33) is not a general solution to the nonlinear and nonholonomic problem. It is probably the case that most, if not all, cases near $\Delta = 0$ arise from interpolation errors, while the small number of cases at large values of Δ probably arise from equation (33) not being a general solution to the problem.

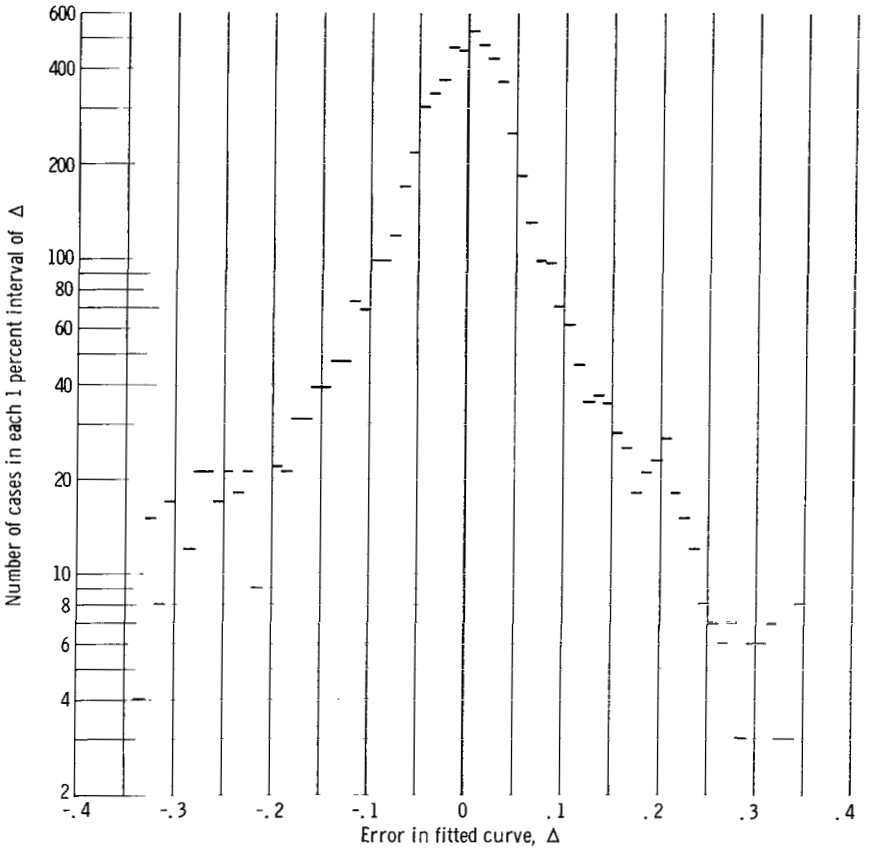

Figure 9. - Number of cases in each 1 percent interval of Δ. Total cases, 6503.

The results of the numerical computation cannot be expected to correspond exactly to the results obtained in real devices for at least two reasons: (1) The definition of adiabaticity, $\Delta M_4 \leq 5$ percent, is an arbitrary one, and there is no a priori reason to expect this particular value of ΔM_4 to be intimately related to whether or not an ensemble of particles are adiabatically confined or not. (2) The magnetic fields assumed in the computations were chosen for mathematical simplicity, and, especially for extreme values of the parameters defining them, do not correspond exactly to actual devices.

Equation (33), while of some intrinsic interest as a particular solution to the mathematical problem of adiabatic particle motion, should not be taken literally as a solution to the physical problem of determining under what conditions nonadiabatic losses will occur. Equation (33) suggests the similarity parameters which will be useful in expressing the results of laboratory experiments on nonadiabatic particle motion, and it also suggests the similarity relations useful in reducing such data. Arguments by induction and analogy are always suspect without direct proof; however, it will be shown subsequently that the experimental results do indeed obey the similarity relations given by equations (27) and (29), but with different values of the numerical constants.

The magnetic fields assumed in this series of computations resemble closely the magnetic fields of axisymmetric devices within the range $0.10 \leq R_c \leq 1.0$ and $\alpha \leq 0.75$. If $\delta \neq 0$, the assumed multipolar field will cease to resemble closely that of real multipolar fields for $r > 0.75\ r_o$. In order to approximate the magnetic fields of specific devices, one must include more terms in the expansion of the A_θ and A_z components of the vector potential.

RESULTS FROM PREVIOUS EXPERIMENTS

Several experiments have been reported in the literature that give information about nonadiabatic particle losses in actual devices. All the experiments except those described in references 1 and 2 yielded information only about nonadiabatic losses that occurred after many reflections between magnetic mirrors.

An excellent study of particle confinement was reported in reference 9 by Gibson, Jordan, and Lauer, who trapped million-electron-volt positrons in the magnetic bottle formed between two current loops. Their apparatus and experimental technique was such that they could not detect the nonadiabatic losses that occurred after a single interaction of the positrons with the magnetic mirrors. They measured the decay of the positron density that resulted from the diffusion of the velocity vectors into the escape region of velocity space. They were able to distinguish between the scattering of the velocity vectors into the escape cone due to collisions with the residual gas in the confinement volume and the faster density decay that resulted from the superposition of nonadiabatic diffusional losses on the losses of collisional origin. Their density decay constants were of the order of seconds, so that the positrons must have made at least 10^8 reflections between the magnetic mirrors of their apparatus before being lost.

The data reported in reference 9 by Gibson, et al. are plotted in figure 10 in terms of the similarity parameters ϵ, R_m, and α. The raw data taken from reference 9 are given in table IV. The investigators observed adiabatic particle motion for the conditions represented by solid circles, and nonadiabatic motion for those conditions represented by open circles. It should be emphasized that even the most nonadiabatic case shown refers to particles that were confined for several seconds on the average. Thus multiple reflection nonadiabatic diffusion into the loss region is a relatively slow process on the time scale of a single reflection between mirrors. For later reference, the best-fit curve for the data of the present experiments is also shown in figure 10.

An experiment similar to that in reference 9 was reported in reference 10 by Rodionov, who also studied the nonadiabatic losses of positrons from a magnetic bottle. In these experiments, it was possible to distinguish between the density decay due to collisions and the faster density decay that resulted when nonadiabatic diffusional losses also

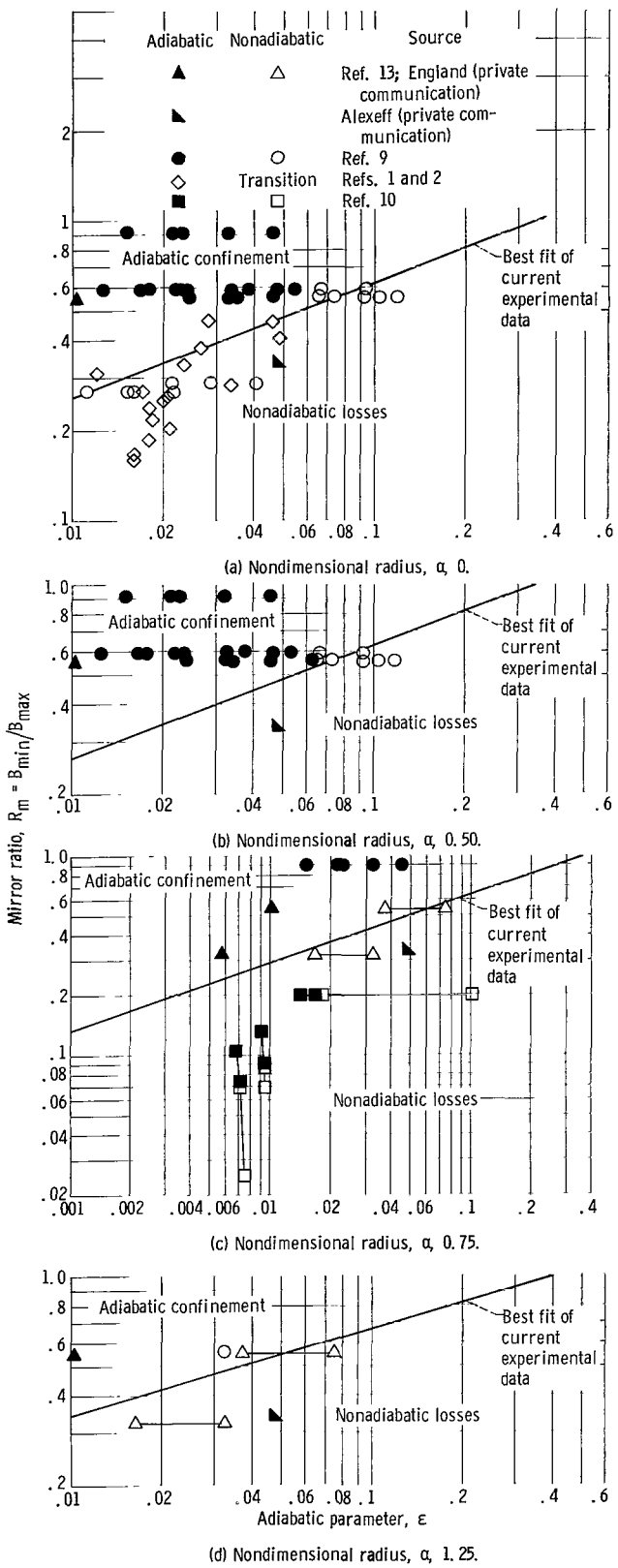

Figure 10. - Prior experimental data for several values of nondimensional radius, α.

occurred. The mirror ratio R_m and the adiabatic parameter ϵ were varied over a relatively wide range of values, although all mirror ratios reported were $R_m \leq 0.2$. Unfortunately, the nature of the apparatus and the experimental technique severely limited the accuracy with which the variables were measured. The energy of the positrons was evidently uncertain by a factor of 3, z_o for the apparatus was uncertain by about 25 percent, and the radial position from which the positrons were lost was known only to be less than the radial position of the apparatus walls. The presumed best values of the variables are shown in table IV. The data for adiabatic motion lie between the solid squares and for nonadiabatic motion between the open squares in figure 10(c). The experimental technique used was such that single interaction nonadiabatic losses could not be detected.

Adiabatic confinement for the conditions listed in table IV has been reported (information received in a private communication with I. Alexeff of the Oak Ridge National Laboratory). These conditions are plotted as the solid right triangles in figure 10. This experiment consisted of energetic electrons trapped between magnetic mirrors. Presumably the only loss mechanism operating in this experiment was collisional scattering into the loss cone, although the method of distinguishing between nonadiabatic and collisional losses was not reported.

England and his colleagues (in ref. 11 and information received in a private communication) have reported the behavior of microwave heated electrons in the "EPA" and "PTF" mirror machines at Oak Ridge. In both machines, there was a core of ≈100-kiloelectron-volt electrons near the axis that appeared to be adiabatically confined, and higher energy electrons - in the million-electron-volt energy range - near the outskirts of the plasma that appeared to be subject to nonadiabatic losses. In this steady-state experiment, it was not clear whether the electrons were lost nonadiabatically after a single interaction with a magnetic mirror, or whether the losses resulted from nonadiabatic diffusion of the velocity vector over many reflections. Each device was operated at a fixed mirror ratio, and the energy of the energetic electrons, which were subject to nonadiabatic losses, was uncertain by about a factor of 2. The experimental parameters are listed in table IV, and the range of values under which nonadiabatic motion was observed is plotted in figure 10, as the open triangles. The solid triangles represent conditions under which adiabatic motion was observed.

The experiments reported in references 1 and 2, unlike the experiments described in the preceding paragraphs, were designed to study a single interaction of a particle with a magnetic mirror. The experimental technique used in these experiments was crude, since it only attempted to measure the conditions under which nonadiabatic losses became large compared with the usual adiabatic losses. The experimental technique was not sufficiently sensitive to measure the onset of nonadiabatic losses, as was done in the series of experiments reported subsequently. The data from references 1 and 2 are listed in table IV and are plotted as diamonds in figure 10(a). These diamonds mark the adiabatic-to-nonadiabatic transition, and correspond to the point between the solid and open symbols in the other experiments. The apparatus used in references 1 and 2 restricted the data to radii very close to the axis of the magnetic field.

It is clear that the previously reported observations on the adiabaticity of particle motion are not sufficiently in agreement with each other or sufficiently complete to test the similarity relation discussed earlier in this report, nor are they adequate to establish adiabatic design criteria over the range of R_m, ϵ, and α of interest in the design of axisymmetric magnetic fields.

EXPERIMENTAL PROGRAM

Apparatus

The incompleteness of the previous experimental results makes it desirable to measure systematically the ϵ appropriate to the adiabatic-to-nonadiabatic transition as a function of the mirror ratio R_m and the average radius at which the particle moves, α.

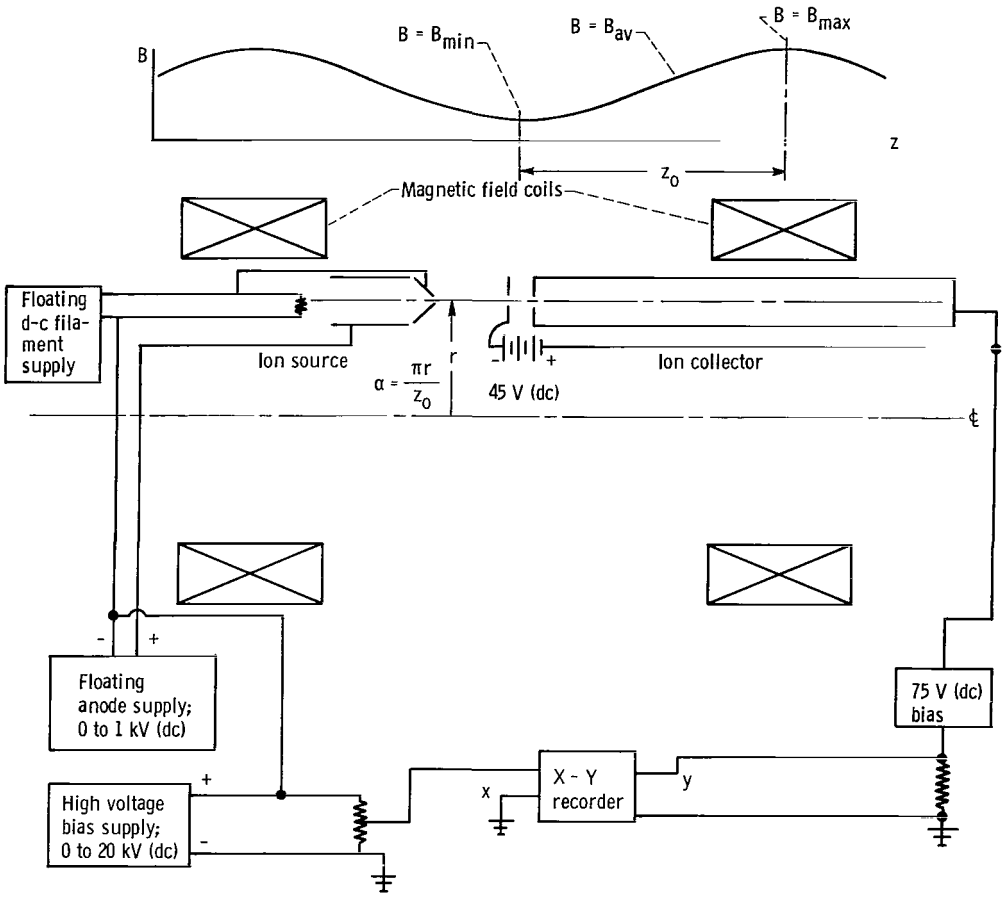

Figure 11. - Schematic diagram of experimental apparatus.

Such a series of experiments was undertaken, subject to the constraint that only axisymmetric geometries could be investigated with the existing apparatus.

The superconducting magnet facility used in this experiment is described in detail in appendix B. The ion source used was a "modified Penning source", similar to that described in reference 12 by Meyerand and Brown. This source has the useful property that it will provide a beam of ions of any gaseous material and can be reconnected to operate as an electron gun. The elements of this ion source are shown in figure 11.

About half the data was taken with singly charged helium ions, whose energy was below 100 electron volts when the ions left the source, and the remainder of the data was taken with electrons. Two runs were made with singly charged neon ions. The ion collector consisted of a Faraday cup 5 centimeters in diameter and 20.3 centimeters long, with a 6.4-millimeter-diameter hole in the end that faced the ion source. A 6.4-centimeter-diameter grounded disk with a 6.4-millimeter-diameter hole was mounted 6.4-millimeters away from the end of the Faraday cup to collect ions that would otherwise impinge on the outer surface of the Faraday cup. The axis of the Faraday cup was

coincident with the axis of the ion source during the taking of data, and this common axis was parallel to the axis of the magnetic field. The ion source and the Faraday cup were mounted on supports that could be positioned at any desired radius in the magnetic field. The background neutral gas pressure was no higher than 5×10^{-7} torr, and the particle currents were in all cases below 10 microamperes. The charged particle densities were too low for collective effects among the particles to have affected the outcome of the experiment.

Procedure

An experimental run was initiated by putting the superconducting coils in the "persistent" mode of operation, in which the currents closed on themselves over a superconducting path, and the magnetic field was constant in time. The axial profile of the magnetic field was measured with a 1-percent-accuracy rotating-coil gauss meter, which was checked against standards both before and after the series of experiments. This profile yielded the experimental parameters z_o, B_{av}, and R_m. The ion source and collector were then positioned at the desired value of α, and the ion source energized. A schematic drawing of the electrical connections of the ion source and collector is shown in figure 11. The Faraday cup was kept biased at +75 volts (dc) to suppress secondary electrons. The ion source could be biased to 18 kilovolts above ground, which provided an electric field between the ion source and the disk in front of the collector. The ion source bias voltage was the effective ion energy, since the ions had energies below 100 electron volts on leaving the source. The y-axis of an X-Y recorder was connected to indicate the current flowing to the collector, while the x-axis indicated the bias voltage, and hence the ion energy.

When the ions entered the Faraday cup, they were no longer acted on by electric fields and interacted only with the magnetic field. Since the diameter of their orbit was in all cases less than the inner diameter of the Faraday cup, and since the length of the cup was in all cases longer than z_o, the ions did not impinge on the inner walls of the Faraday cup unless the velocity vector of the particle happened to lie in the escape cone.

The adiabatic theory of particle reflection from a magnetic mirror states that the angular opening of the escape cone in velocity space is a function only of the mirror ratio R_m

$$\theta_1 = \sin^{-1} R_m^{1/2} \tag{35}$$

When ϵ becomes sufficiently large, however, the escape cone angle becomes larger than θ_1, and nonadiabatic losses are said to occur. In the present series of experiments, all

variables except the ion energy were held constant during a given run. Ions were accelerated to a given energy, entered the Faraday cup, interacted with the magnetic field, and a certain fraction were reflected back out the same 6.4-millimeter-diameter hole through which they entered. In the adiabatic regime of operation, the fraction of particles reflecting back out of the collector is independent of the ion energy and hence independent of ϵ. As the energy is increased to the point where nonadiabatic motion begins, the escape cone opens up, and fewer particles are reflected back out the hole in the collector. The indicated ion current to the collector will therefore be a constant up to a critical energy, corresponding to point A in figure 1 (p. 2), and will then increase.

This behavior is illustrated in figure 12, which is one of the X-Y recordings that form the raw data of this experiment. In the region below about 4 kilovolts, the collected ion current is constant, so that the escape cone angle is not a function of energy. Above 4 kilovolts, however, the collected ion current is a ramp function, which indicates that the escape cone angle was opening up as the particle energy (and hence ϵ) was increased. The energy at which the ion current is no longer a constant is the "critical" energy, above which nonadiabatic losses occur. The experimental conditions under which these critical energies were measured are listed in table V. If a device is to contain particles adiabatically, the particle energy should be below this critical energy. It should be noted that this experimental technique gives information about only a single interaction with the magnetic barrier.

Results

The raw experimental data were converted to the nondimensional similarity parameters ϵ, R_m, and α. The experimentally obtained values of ϵ, corresponding to the critical energy, have been plotted as a function of R_m in figure 13, for eight values of α, $0 \leq \alpha \leq 1.75$. The same similarity relation is obtained that was used in correlating the numerical results

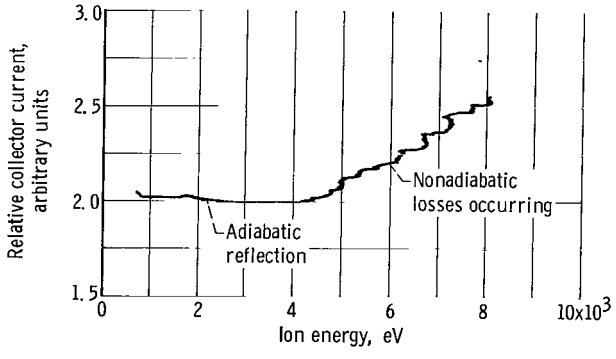

Figure 12. - Raw data from X-Y recorder. Nondimensional radius, α, 1.75.

$$R_m = \left(\frac{\epsilon}{\epsilon_1}\right)^{A_1} \tag{36}$$

although the correlation involves the mirror ratio R_m rather than R_c, and the values of A_1 and ϵ_1 are different. The experimental data for each value of α were substituted into the same curve-

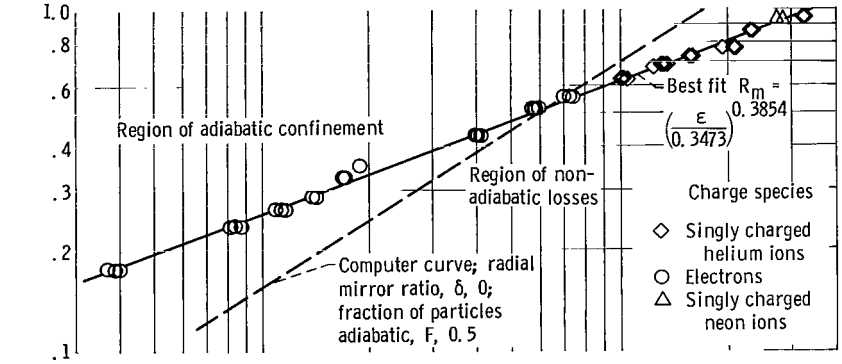

(a) Nondimensional radius, α, ≅ 0.

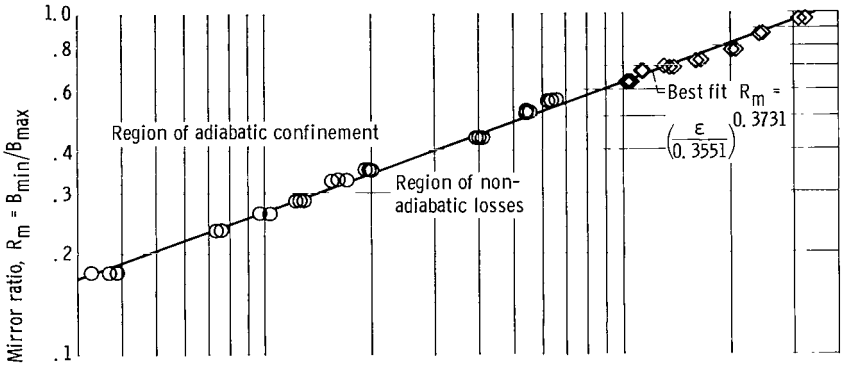

(b) Nondimensional radius, α, 0.25.

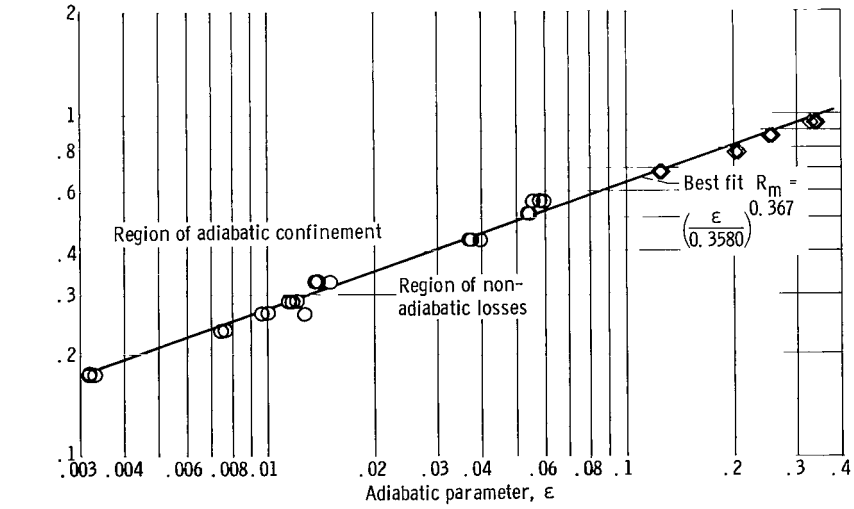

(c) Nondimensional radius, α, 0.50.

Figure 13. - Experimental data for several values of nondimensional radius.

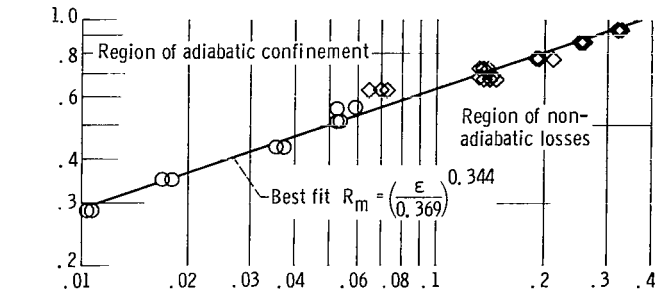

(d) Nondimensional radius, α, 0.75.

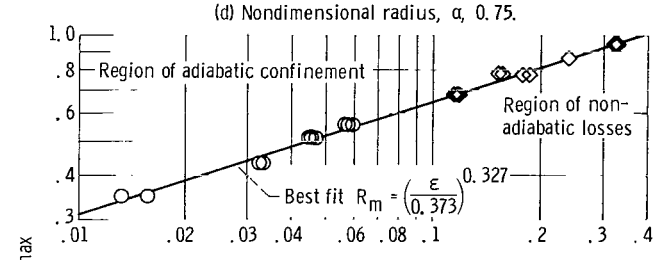

(e) Nondimensional radius, α, 1.00.

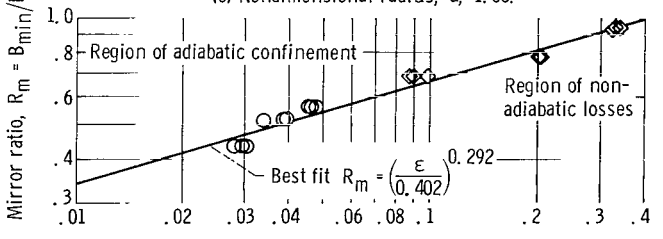

(f) Nondimensional radius, α, 1.25.

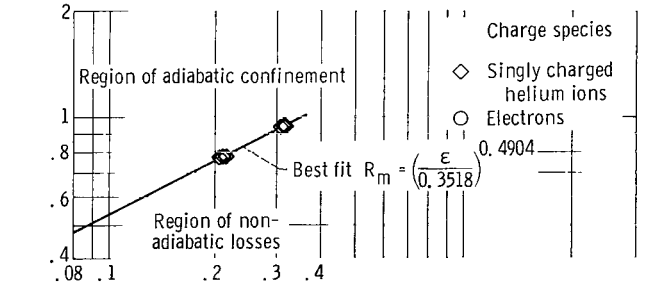

(g) Nondimensional radius, α, 1.50.

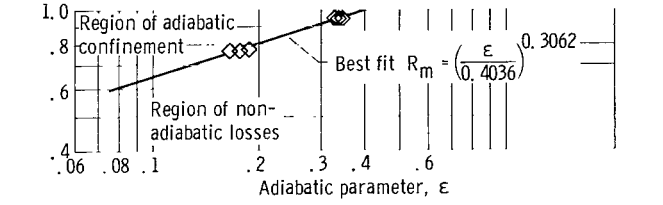

(h) Nondimensional radius, α, 1.75.

Figure 13. - Concluded.

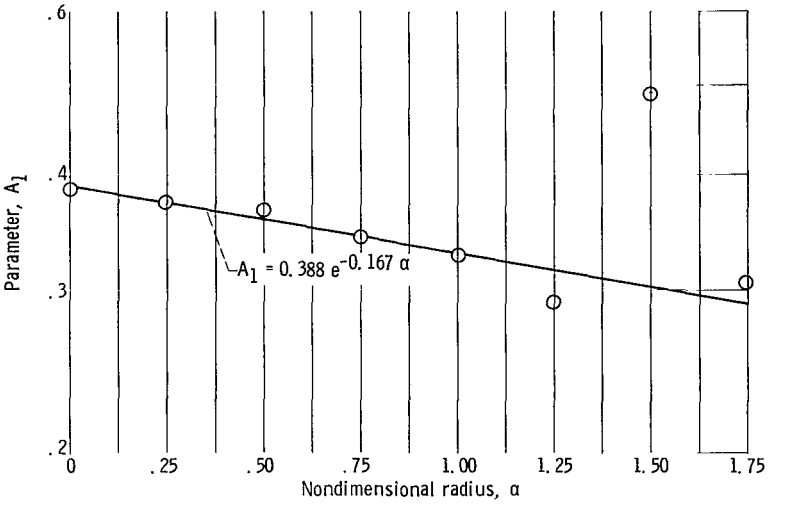

Figure 14. - Parameter A_1 from experimental curves as function of nondimensional radius α.

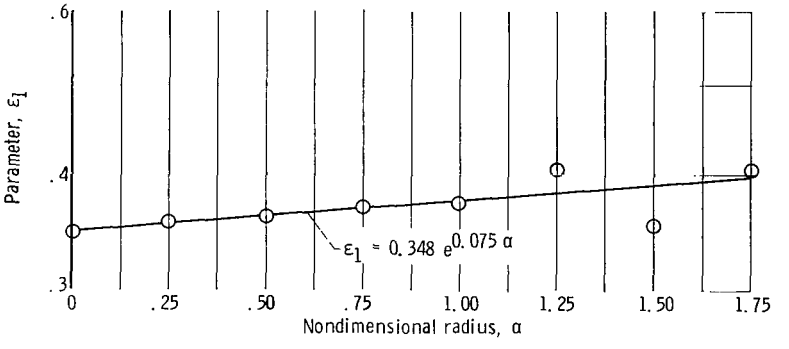

Figure 15. - Parameter ϵ_1 from experimental curves as function of nondimensional radius α.

fitting computer program used to fit the analytical results. The straight lines on these log-log plots are the least-squares fit to the logarithms of the experimental data. The constants A_1 and ϵ_1 are listed in table VI(a) for each value of α for which data were taken.

The parameter A_1 from the experimental curves is shown plotted as a function of α in figure 14. The parameter A_1 can be correlated by the relation

$$A_1 = A_{1o} e^{P_1 \alpha} \tag{37}$$

where, for the present experiment, $A_{1o} = 0.388$, and $P_1 = -0.167$. The parameter ϵ_1 for the experimental data is shown plotted as a function of α in figure 15 and can be correlated by the relation

$$\epsilon_1 = \epsilon_{1o} e^{P_2 \alpha} \tag{38}$$

where, for the present experiment, $\epsilon_{1o} = 0.348$, and $P_2 = 0.075$. The anomalous point at $\alpha = 1.50$ was discarded in both correlations, since it was based on many fewer experimental points than those for which $\alpha \leq 1.00$. The results of the current series of experiments can be summarized in analytic form by the statement that single interaction nonadiabatic losses will not occur in axisymmetric geometries if

$$R_m \geq \left(\frac{\epsilon}{0.348\, e^{0.075\, \alpha}} \right)^{0.388\, e^{-0.167\, \alpha}} \tag{39}$$

where the experimental results are represented by the equality sign.

Comparison of the experimentally derived similarity relation of equation (39) with equation (33), which was used to correlate the analytical results, requires that the mirror ratio R_m be transformed to R_c. Since $R_m = R_c$ when $\bar{\alpha} = 0$, one can show, with the help of equation (21), that

$$R_c = \frac{R_m - \gamma}{1 - R_m \gamma} \tag{40}$$

where

$$\gamma = \frac{I_0(\bar{\alpha}) - 1}{I_0(\bar{\alpha}) + 1} \tag{41}$$

The experimental values of R_m were transformed according to equation (40), and the experimental data obeyed the similarity relation of equation (27). The values of A and ϵ_o from the transformed experimental data curves are listed in table VI(b). The parameter A for the experimental curves is plotted as a function of α in figure 16.

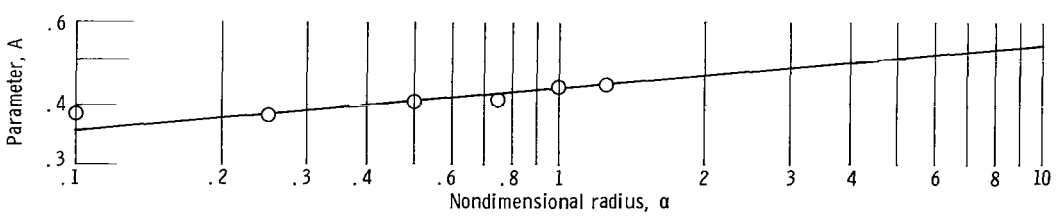

Figure 16. - Parameter A from transformed curves of mirror ratio R_c at nondimensional radius of particle α, as it passes through minimum magnetic field B, as function of nondimensional radius α.

These values of A are consistent with the power-law similarity relation of equation (29), which was used to correlate the analytical results.

Within the limitations of the data, one may conclude that the analytical problem considered in the section NUMERICAL ANALYSIS and the preceding experimental results are both correlated by the same similarity parameters and by the similarity relation of equation (27). It therefore appears from this series of experiments that the similarity relations and the similarity parameters appropriate to the problem of nonadiabatic particle motion have been established, and that the constants have been found for the axisymmetric geometry. The fact that the experimentally determined critical values of ϵ for electrons and singly charged helium and neon ions fall along the same similarity relation is further evidence in support of this result.

The measurement of the magnetic field profile yielded values of R_m and B_{av} that could not have had errors of more than 3 percent. The error in z_o may have been as great as 5 percent in some cases. The error in measuring the particle energy could have been as great as 10 percent. These errors give rise to error limits on ϵ of $\Delta\epsilon = \pm 15$ percent. The average error in the radial position was $\Delta\alpha \approx \pm 0.15$, a fixed rather than a proportional error. This error arose from a 0.31-centimeter uncertainty in the radial position of the ion beam, due to the 0.64-centimeter hole in the ion source and collector, and an additional 0.64-centimeter uncertainty in the position of the ion source and collector axis. The range of the principal experimental variables was $0 \leq \alpha \leq 1.75$, $0.175 \leq R_m \leq 0.945$, $0.059 \leq z_o \leq 0.241$ meter, $1/1837 \leq m \leq 20$ atomic mass units, $0.029 \leq B_{av} \leq 1.89$ webers per square meter, and $1500 \leq V \leq 7800$ electron volts.

CONCLUSIONS

Modes of Nonadiabatic Particle Loss

In the INTRODUCTION, nonadiabatic particle losses were divided into two classes: (1) nonadiabatic losses due to enlargement of the escape cone, which result after a single interaction of a particle with a magnetic barrier, and (2) nonadiabatic losses that occur after many reflections, which result from a random-walk diffusion of a particle across the boundary of the enlarged escape cone. The first nonadiabatic loss mechanism was observed in the numerical computations of Garren, et al. (ref. 4), in the experimental results reported in references 1 and 2, and in the results of the present series of experiments, which employ an experimental technique that demonstrates this mode of nonadiabatic loss. The second mode of nonadiabatic loss was observed in the experiments of Gibson, et al. (ref. 9), and of Rodionov (ref. 10). In both experiments, the positrons confined in their apparatus were lost after approximately 10^8 reflections. The division

of nonadiabatic losses into single reflection and multiple reflection losses may be regarded as experimentally established.

Comparison of Present Results with Previous Experiments

The data of the present experiment map out the critical conditions for which nonadiabatic losses will start to occur. No other experiment therefore is expected to have detected nonadiabatic motion to the upper left of the present experimental curves, nor would adiabatic motion be expected to the lower right of these curves. In figure 10, however, are several instances of disagreement with the present experiment. These will be examined.

The adiabatic-to-nonadiabatic transitions reported in references 1, 2, 10, and a private communication with Alexeff all lie below the transition line determined in the present experiment. This discrepancy could be explained in part by the inaccuracy with which the experimental variables were measured, but the most probable source of the discrepancy is that these experiments measured a somewhat different phenomenon than the present experiments.

In the experiment of Alexeff electrons were heated by microwave energy, and the experiment was steady-state. The disagreement with the present results probably arises from the fact that the electrons in Alexeff's apparatus possessed velocity components in the vicinity of point C in figure 1 (p. 2), and the loss cone was actually much larger than the adiabatic loss cone. The electrons with velocity vectors to the left of point C will appear to be adiabatically confined, and the large number of nonadiabatic losses would go undetected because of an inability to distinguish between electrons escaping in the adiabatic loss cone, and electrons escaping in the large nonadiabatic loss region.

The adiabatic-to-nonadiabatic transition region determined in the experiments of Rodionov (ref. 10) does not agree with the findings of the present experiment. This discrepancy could be explained on the same basis as that of Alexeff's experiment. This discrepancy could also be explained by the large limits of error on the variables of this experiment.

The experimental technique used in references 1 and 2 did not detect the onset of nonadiabatic particle motion, but it did detect instead the energy at which the largest number of particles became nonadiabatic. The velocity corresponding to this energy lies in the vicinity of point B in figure 1. If Φ is the flux of particles escaping as a result of nonadiabatic effects and θ is the escape cone angle, the experimental technique of references 1 and 2 was such as to detect

$$\left.\frac{\partial \Phi}{\partial \theta}\right|_{OABC} = \text{maximum} \tag{38}$$

rather than the transition measurement of the present experiment

$$\left.\frac{\partial \Phi}{\partial \theta}\right|_{OABC} = \text{nonzero} \tag{39}$$

All but two of the diamonds in figure 10(a), which represent the transition energy determined in the experiment of references 1 and 2, lie below the transition line of the present experiment. This is to be expected, since the ϵ appropriate to point B is larger than that appropriate to point A.

The observations of England (ref. 11 and a private communication) are consistent with the results of the present experiments, in view of the uncertainty in the energy of the nonadiabatic particles. The experiments of Gibson, et al. (ref. 4) show good general agreement with the present series of experiments, with one interesting and significant exception. It should be noted in figures 10(a) and (b) that the adiabatic-to nonadiabatic transition, as reported by Gibson, et al. (ref. 9), lies at slightly smaller values of ϵ than the present experimental results. Evidently this experiment was sensitive and accurate enough to detect the nonadiabatic diffusional losses from points in velocity space only slightly above and to the right of point A in figure 1 (p. 2). The small discrepancy between the present experiment and the results reported by England and by Gibson, et al. (ref. 9) may also be due to relativistic effects, since the particles in these latter experiments were relativistic.

Comparison of Experimental Results with Numerical Computations

Although the numerical and experimental results obey the same similarity relation, the numerical constants in the similarity relation are different and yield different slopes and intercepts. In the particular case $\alpha = 0$, shown in figure 13 (pp. 25 and 26), the numerical and experimental curves cross in the vicinity of $R_m = 0.515$ for $F = 0.5$ adiabatic and $\delta = 0$. At this mirror ratio, at least some particles are lost when their adiabatic invariant M_4 varies by about 5 percent during a single interaction with the magnetic mirror. In the range $0.515 \leq R_m \leq 1.0$, the experimental points lie to the right of the numerical curve, suggesting that, in this region, nonadiabatic losses occur only if M_4 varies by more than 5 percent during a single interaction with the magnetic mirror field. In the range $0 \leq R_m \leq 0.515$, nonadiabatic losses will occur if M_4 varies by less than 5 percent during a single interaction with the magnetic mirror.

Sample Computations

The implications of the numerical results may be best appreciated by applying them

to a specific example. A "reference device" was chosen for purposes of illustration, whose characteristics are shown in figure 17 and listed as follows:

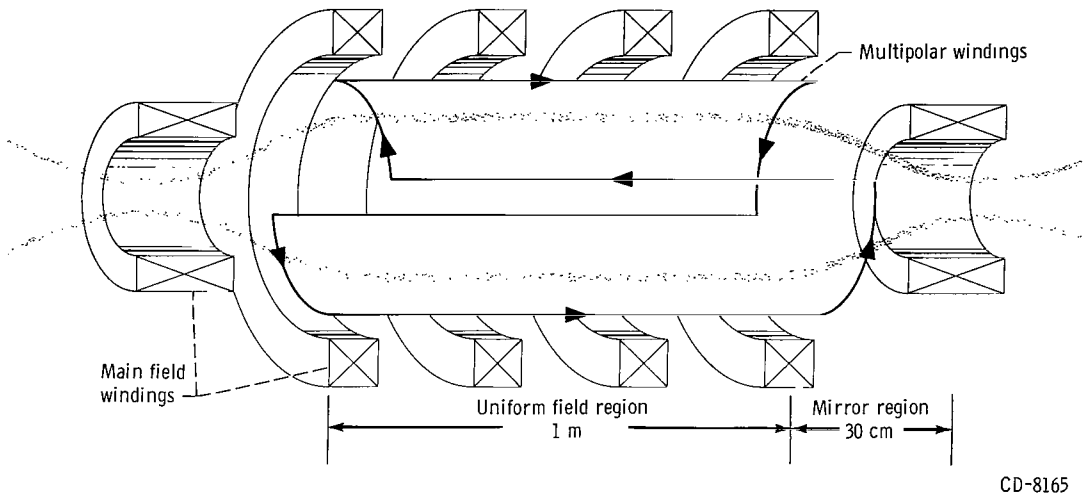

Figure 17. - Characteristics of reference apparatus.

Confined particle species, A = 2	Deuterium
Length of uniform field region, cm	100
Length of mirror region, z_o, cm	30
Minimum magnetic field, B_{min}, kG	75
Maximum magnetic field, B_{max}, kG	150
Reference mirror ratio, $R_m = B_{min}/B_{max}$	0.50
Plasma radius (maximum $\alpha_{max} \approx 0.50$), r_p, cm	5
Radius of multipolar windings ($\delta \approx 0.75$), r_o, cm	9
Number of multipolar conductor pairs (quadrupole), n	2
Radial mirror ratio ($\delta \approx 0.75$) at r = 2 cm	1.05

The reference device is intended to be typical of the next technological generation of minimum-B controlled fusion research devices, in which the magnetic fields and particle energies, but not the dimensions, of eventual fusion reactors are achieved. In the following discussion, the characteristics of the reference device are varied one by one, and the effects of these variations on the critical energy are determined.

Figure 18 is a plot of the critical energy (based on F = 0.5 adiabatic, and a 5-percent variation of M_4) as a function of δ, the radial mirror ratio. The critical energy is a monotonically decreasing function of δ, which implies that the addition of multipolar windings to the axisymmetric mirror configuration causes a particle to become less adiabatic, and hence more likely to be lost from the device. This general trend of adiabaticity with δ is true, in general, over the range studied in the numerical computa-

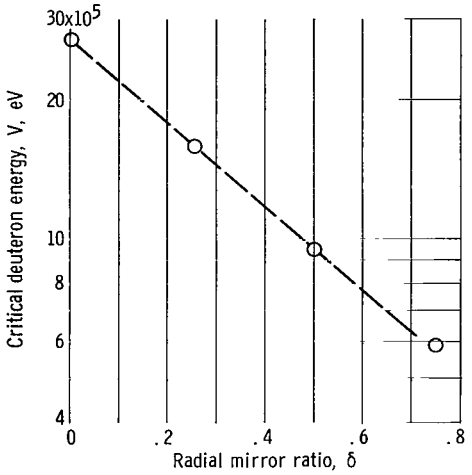

Figure 18. - Critical energy V as function of radial mirror ratio δ in reference device. Multipolar currents, n, 2; nondimensional radius, α, 0.50; fraction of particles adiabatic, F, 0.5; mirror ratio, R_c, 0.50.

tions. Adiabatic confinement is therefore apt to be even more of a problem with minimum-B geometries than with axisymmetric magnetic bottles. The physical reasons for this decrease of adiabaticity are fairly clear: the addition of multipolar windings increases the uneveness of the magnetic field. The effect of small bumps, or sharp gradients, on nonadiabatic losses has been illustrated in the experiments of Brevnov and Tomashchuk (ref. 13).

Figure 19 is a plot of the critical energy as a function of the mirror ratio of the reference device. In this computation, it was assumed that B_{min} and B_{max} were adjusted in such a way that B_{av} was kept constant at 11.25 webers per square meter. The dashed line is taken from the numerical computations. The solid line is taken from the experimental results, which were for $\delta = 0$, and is equivalent to operating the reference device with the multipolar windings turned off. A change of a factor of 2 in the mirror ratio of the reference device will change the critical energy by about a factor of 100. Alternatively, a change in particle energy of a factor of 2 will cause a change of about 11 percent in the critical mirror ratio. This suggests that the choice of the maximum energy and/or mirror ratio should be a matter for careful study.

Figure 20 is a plot of the critical energy of the reference device as a function of n, the number of pairs of multipolar current-carrying windings. As one can see, the critical energy is a monotonically increasing function of n, suggesting that, as the number of pairs of windings is increased, the motion of a particle at a given radius will become

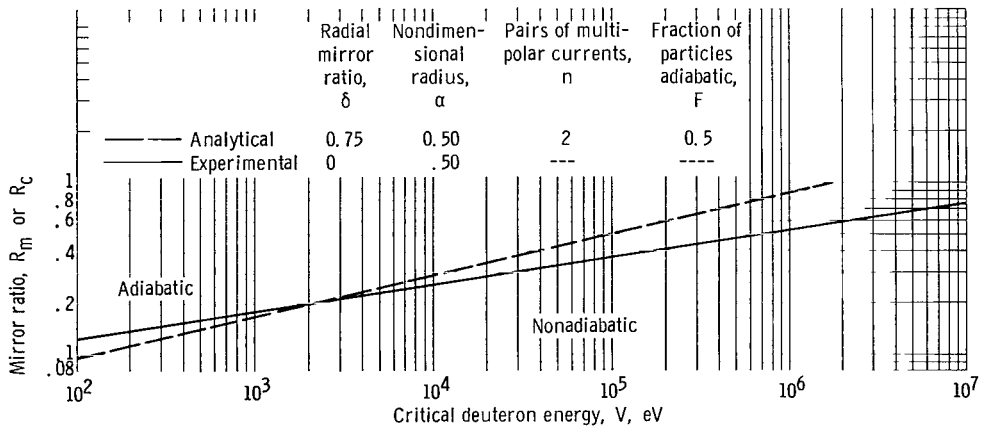

Figure 19. - Critical deuteron energy V as function of mirror ratio R_m or R_c for reference device.

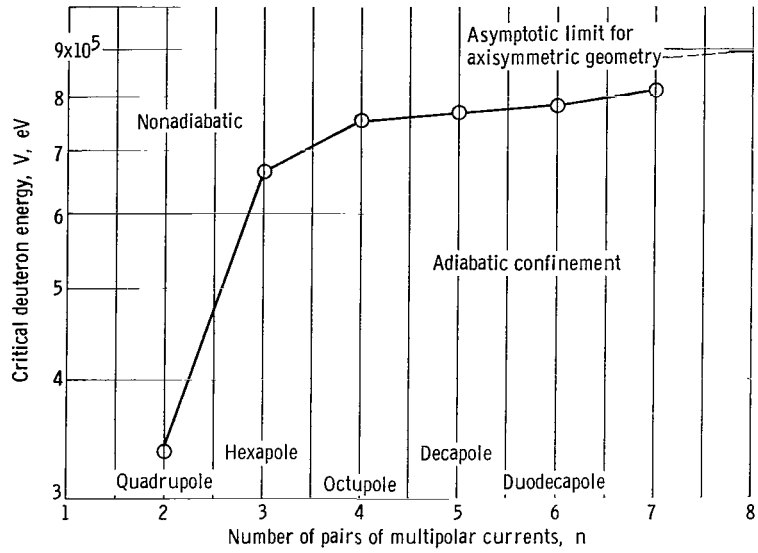

Figure 20. - Critical deuteron energy V as function of number of pairs of multipolar currents n in reference device: radial mirror ratio, δ, 0.75; multipolar currents, n, 2; nondimensional radius, α, 0.50; fraction of particles adiabatic, F, 0.50.

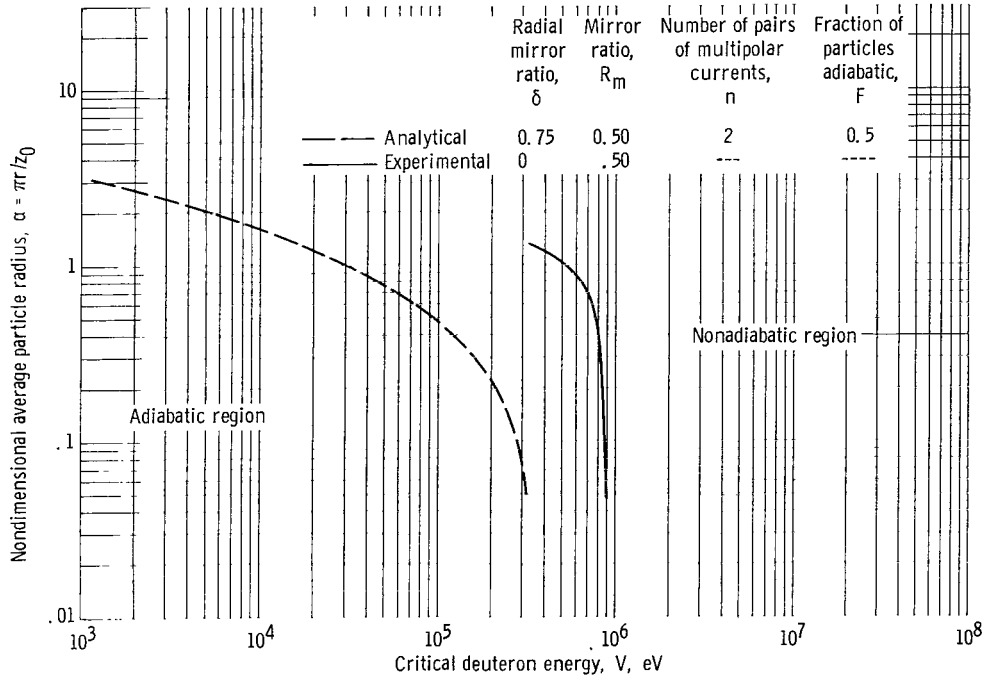

Figure 21. - Critical deuteron energy V as function of nondimensional average particle radius α for reference device.

more adiabatic. This result is reasonable on physical grounds, since the multipolar field increases with radius as

$$B_m \sim \left(\frac{\alpha}{\alpha_o}\right)^{n-1}$$

so that, at a given radius, the multipolar field for large n is not as great as it is for small n. For large n, the unevenness in the magnetic field at a given radius is relatively small, and approaches the characteristics of an axisymmetric field as a limit. For small n, the multipolar field is relatively larger, and produces a relatively larger perturbation in the motion. This trend of adiabaticity with n is a general one and is not confined to the reference device.

Figure 21 is a plot of the critical energy as a function of the average nondimensional radius at which the particle moves. The dashed line is based on the numerical computations; the solid line is a consequence of applying the experimental results to the reference device, but with $\delta = 0$. One may see that there is a broad region in the vicinity of the axis where the critical energy is relatively constant, followed by a monotonic decrease with radius. This result is general, and comes about because the magnetic field is relatively constant near the axis and becomes more nonuniform only at larger radii. The general behavior shown in figure 21 is in good agreement with the observations of Gibson, et al. (ref. 9), who measured nonadiabatic losses at several radii and reported that they observed no significant change in the nonadiabatic losses until relatively large radii were investigated.

Virtually all the numerical computations were made for an azimuthal injection angle of $\theta = 0$, a position between the Ioffe bars. Table VII shows the critical energy for five different values of θ for the reference device. One may see that the particular angle chosen corresponds to the most nonadiabatic behavior, so that equation (33) together with the constants of tables II and III represents the worst or most nonadiabatic behavior that would be expected in the minimum-B configuration assumed in this investigation.

Present Experimental Results as Engineering Design Criteria

The experimental results given earlier can serve as criteria for the design of axisymmetric magnetic mirrors that will suffer no nonadiabatic particle losses. In the present series of experiments, the conditions for which nonadiabatic losses start to occur have been measured for a single interaction of a particle with a magnetic barrier. To confine the maximum number of particles that the adiabatic theory allows, the apparatus should

operate under conditions that lie above and to the left of the lines in figures 13 and 14 (pp. 25, 26, and 27). If the nonadiabatic losses caused by multiple reflection diffusion of the velocity vector are to be avoided, the data of Gibson, et al. (ref. 9) indicate that the values of R_m should be about 8 percent higher than the value of R_m given by the present single reflection experiments. Since large values of ϵ generally imply more economical apparatus and better satisfaction of the finite radius of gyration stabilization criterion, the apparatus should be designed as close to this value of ϵ as possible.

Since the magnetic field is less uniform away from the magnetic field axis, the value of R_m defining the critical adiabatic-to-nonadiabatic conditions off axis will be greater than the value of R_m for $\alpha = 0$. For this reason, a given piece of apparatus should be designed to be adiabatic at the maximum anticipated plasma radius, and particles moving at smaller radii will automatically be adiabatic. The preceding experimental results were obtained in an axisymmetric magnetic field and must be applied with caution to the minimum-B fields used in the numerical computations. If these results are used as design criteria for minimum-B geometries, it should be realized that the superposition of a multipolar field on an axisymmetric mirror field will make the combined geometry less adiabatic. The experimental results of equation (39) should therefore be regarded as an upper bound on ϵ, or a lower bound on R_m, the exceeding of which will certainly result in nonadiabatic losses from the combined geometry. Since experimental design criteria for minimum-B geometries are not yet available, machines with such geometries should be designed to lie as far as possible above and to the left of the curves in figure 13. The magnetic field near the axis of a combined geometry is similar to that in an axisymmetric field alone, so that the results of the present experiments for $\alpha = 0$ should be capable of being carried over virtually intact for particles close to the axis of a combined field. As larger radii, larger values of n, and larger values of the radial mirror ratio δ are considered, the R_m of the combined field should be designed to be further and further above that given by equation (39). The quantitative effects of δ and n on the adiabatic-to-nonadiabatic transition line remain to be investigated in a further series of experiments.

Implications of Present Results for the Problem of the Self-Sustainability of a Fusion Reaction

It would be most desirable if eventual fusion reactors were self-sustaining, that is, if the charged reaction products could be confined in the reaction volume until they have transferred their energy to the fuel ions, thus making external heating and injection of the fuel unnecessary.

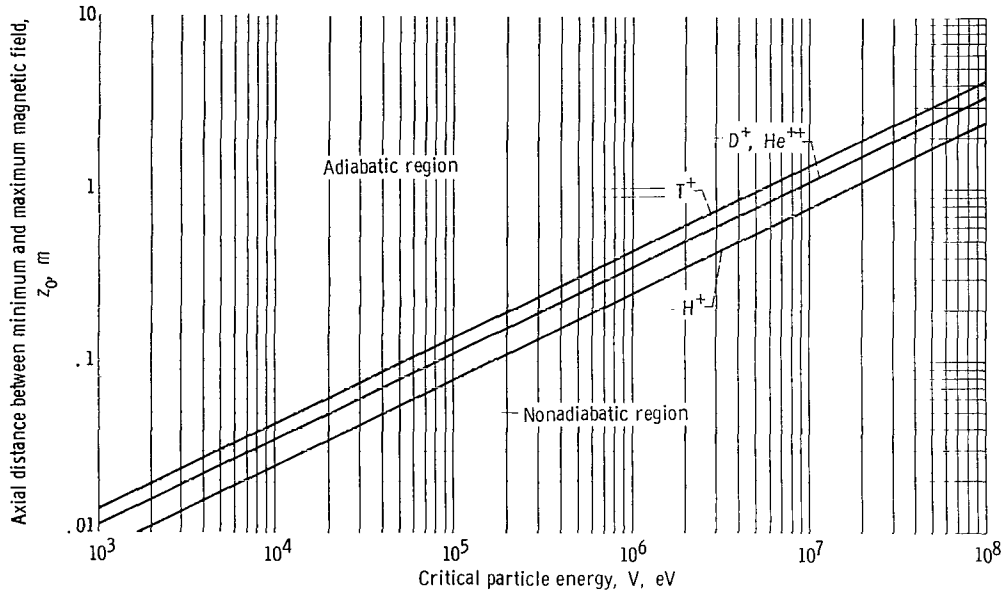

Figure 22. - Critical particle energy V as function of apparatus dimensions for reference device. Nondimensional radius, α, 0.

Two of the difficulties in the way of a self-sustaining fusion reactor are (1) the energetic reaction product may be scattered by collisions into the escape cone before it gives up a significant fraction of its energy to the fuel and (2) the reaction product may be lost nonadiabatically before it can give up a significant fraction of its energy to the fuel. Only the latter question, whether it is reasonable to expect these reaction products to be adiabatically confined, will be considered.

The charged reaction products of a thermonuclear reactor include doubly charged helium 3 and helium 4 and singly charged hydrogen, which have energies in the range $1 \leq E \leq 15$ million electron volts. The critical energy is plotted in figure 22 as a function of z_o, the characteristic dimension of the magnetic field, which is predicated on the assumptions $\alpha = 0$, $\delta = 0$, $R_m = 0.5$, and $B_{av} = 11.25$ webers per square meter. The experimental data of figure 13 have been used as design criteria. The three reaction products listed are shown in figure 22. It can be seen that, if the fusion reactor has a value of z_o of more than about $1\frac{1}{2}$ meters, the reaction products will be adiabatically confined. Since a full-scale fusion reactor would probably have dimensions at least this large, it is reasonable to conclude that nonadiabatic losses need not prevent a fusion reactor from being self-sustaining.

Lewis Research Center,
National Aeronautics and Space Administration,
Cleveland, Ohio, September 1, 1965.

APPENDIX A

SYMBOLS

Unless otherwise noted, the rationalized mks system of units is used in this report.

A	exponent of similarity relation
A_o	parameter used in eq. (29)
A_{oA}	parameter used in eq. (30)
A_z	axial component of magnetic vector potential
A_θ	theta component of magnetic vector potential
$\underline{A}$	magnetic vector potential
A_1	parameter used in eq. (37)
A_{1o}	parameter used in eq. (37)
B	magnetic field strength
B_{av}	average magnetic field, $1/2(B_{min} + B_{max})$
B_m	multipolar magnetic field at multipolar current sheet
B_{max}	maximum magnetic field strength on axis
B_{min}	minimum magnetic field strength on axis
C_1	constant defined by eq. (9)
C_2	constant defined by eq. (21)
C_3	constant defined by eq. (22)
C_4	parameter used in eq. (28)
C_5	parameter used in eq. (28)
C_6	parameter used in eq. (30)
C_7	parameter used in eq. (31)
E_1	parameter used in eq. (28)
E_2	parameter used in eq. (28)
F	fraction of particles adiabatic
$\underline{i_z}$	unit vector in z-direction
$\underline{i_\theta}$	unit vector in θ-direction
j	current per unit length
K	parameter used in eq. (29)
K_o	parameter used in eq. (31)
L	Lagrangian, given by eq. (14)
M_4	adiabatic invariant, defined by eq. (1)
m	ion mass
n	number of pairs of multipolar currents
P_1	parameter used in eq. (37)
P_2	parameter used in eq. (38)
R_c	mirror ratio at radius $\bar{\alpha}$, defined by eq. (11)
R_ℓ	average radius of gyration of particle, defined in eq. (3)
R_m	mirror ratio, B_{min}/B_{max} on magnetic field axis
r	radial position
r_o	radial position of multipolar windings
r_p	plasma radius, m

T dimensionless kinetic energy, given by eq. (25)

t time

V particle energy, eV

v total velocity of particle

$v_\perp$ particle velocity perpendicular to magnetic field

$v_{||}$ particle velocity parallel to magnetic field

z axial coordinate

z_o axial distance between B_{min} and B_{max}

α nondimensional radius, $\pi r/z_o$

α_o nondimensional radial position of multipolar windings, $\pi r_o/z_o$

$\overline{\alpha}$ nondimensional radius of a particle as it passes through B_{min}

γ parameter defined by eq. (41)

Δ defined by eq. (34)

δ radial mirror ratio, defined by eq. (24)

ϵ adiabatic parameter, defined by eq. (3)

ϵ_o constant appearing in similarity relation

ϵ_1 parameter used in eq. (38)

ϵ_{1o} parameter used in eq. (38)

η dimensionless axial coordinate, $\pi z/z_o$

θ escape cone angle

θ_1 angle defined by eq. (2)

μ_o permeability of free space, 4π $4\pi\times10^{-7}$ H/m

τ dimensionless time, defined by eq. (15)

Φ flux of particles lost through magnetic mirror

χ dimensionless generalized coordinate

ω angular frequency

APPENDIX B

EXPERIMENTAL APPARATUS

Superconducting Coils

The fields of cryogenic engineering and superconductivity have recently matured to the point where superconducting magnetic field coils can be built and operated as a facility for research in other areas. A split pair of superconducting coils with a maximum field of 2.5 webers per square meter on the axis and an accessible diameter of 17.8 centimeters has recently been placed into service. The coils are operated in a magnetic bottle configuration that may be either symmetric or asymmetric about the midplane. The mirror ratio of a symmetric configuration may be altered by varying the spacing of the coils. A normalized plot of the field along the axis with both coils symmetrically energized is shown in figure 23.

Each coil contains approximately 26 kilometers of 0.25-millimeter-diameter niobium - 25 percent zirconium wire plated with 0.025 millimeter of copper on the radius and covered with an additional 0.025 millimeter of enamel insulation.

The critical current of the wire utilized was greater than 28 amperes in a small test coil (850 G/A). The average operating current, however, was set at 14.7 amperes to allow for nonuniform wire quality and collective degradation effects. With this current, the maximum field of both coils was just 2.5 webers per square meter on the axis before transition to the normal state. The time required to bring the two coils up to rated field when operated in series is 150 minutes. At the present time, both coils have withstood six normal transitions while installed in their respective Dewars.

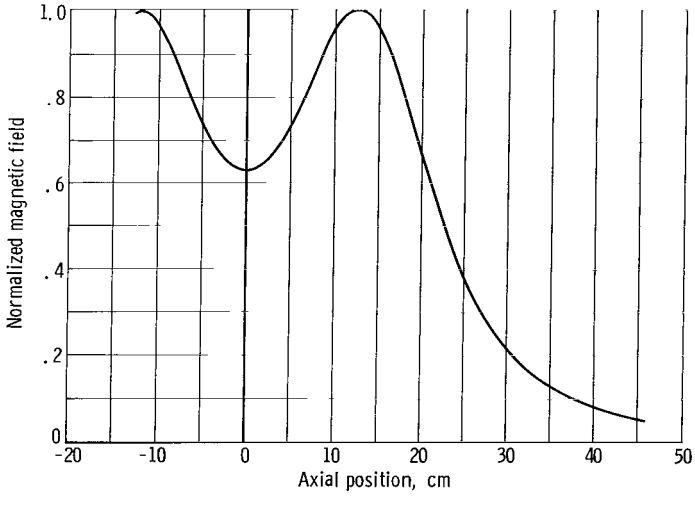

Figure 23. - Normalized magnetic field profile with 6-inch spacers between coils. Maximum magnetic field strength, 23 kilogauss.

Magnet Dewars

Each of the two superconducting coils is enclosed in a multilayer Dewar whose outside dimensions are 12 centimeters in thickness along the coil axis, and 51.7 centimeters by 74.5 centimeters in a plane normal to the coil axis. Each Dewar consists of an inner stainless-steel canister that encloses the superconducting coils and a 9.90-liter liquid-

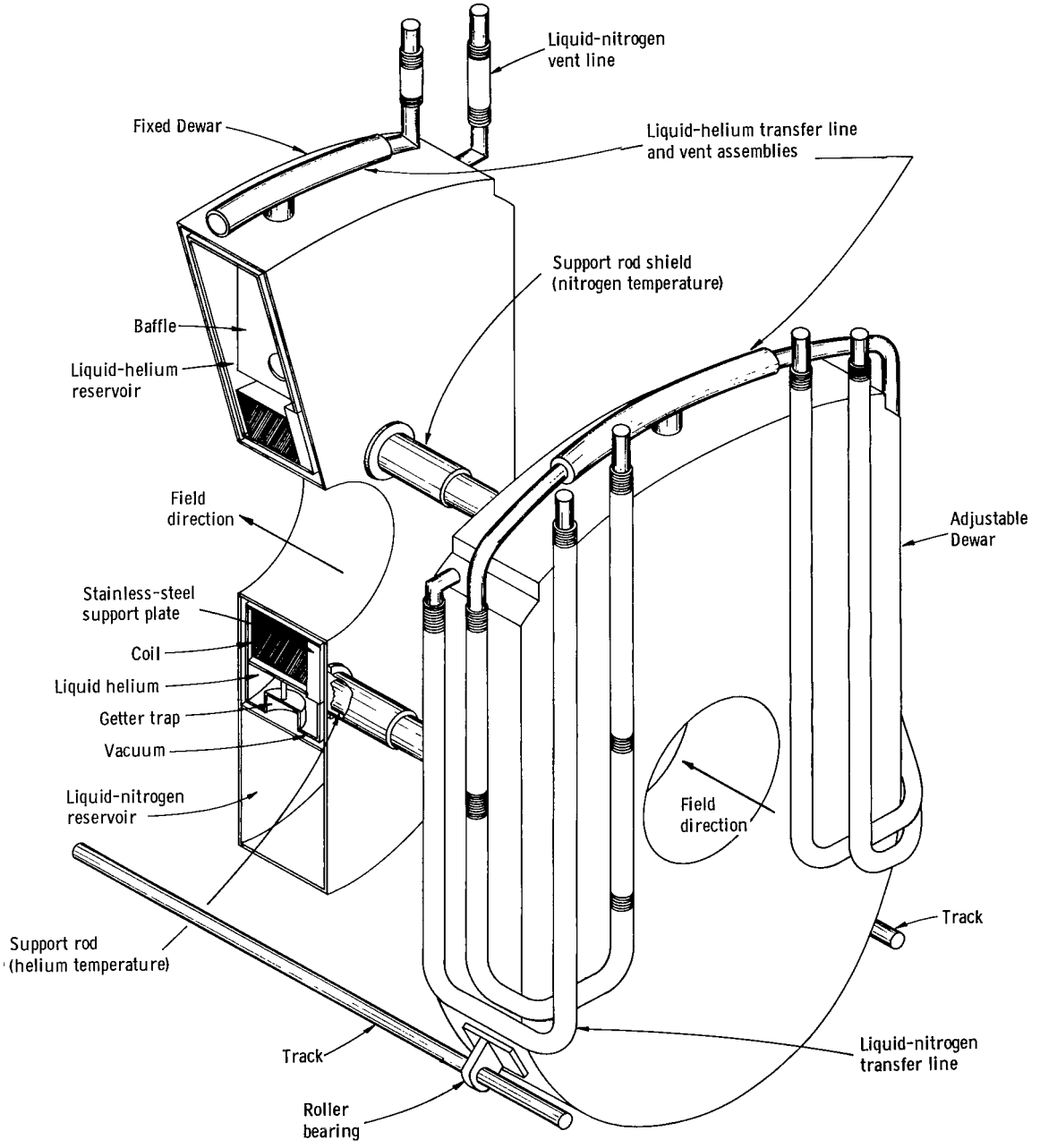

Figure 24. - Cutaway drawing of coil Dewars.

helium reservoir, and an outer aluminum canister that contains a 10.60-liter-reservoir for liquid nitrogen. All seams in the Dewar are vacuum-tight welds. The outer surface of the liquid-nitrogen canister is exposed to the vacuum in which the experiment is performed and serves as a liquid-nitrogen cold trap. An isometric cross section of the Dewars and coils is shown in figure 24.

The unobstructed working diameter is 17.8 centimeters in the Dewar and 26.6 centimeters in the space between the Dewars. An end view of the Dewar assembly is shown in figure 25. The heat leak into the liquid-nitrogen and liquid-helium canisters of each Dewar is shown in table VIII along with the operating time between fillings of the canisters.

Approximately 4 hours are required to cool the coils from room temperature and to fill all the canisters. Approximately 130 liters of liquid helium are required to cool the two coils from liquid-nitrogen temperature to liquid-helium temperature and to fill both canisters. The helium vent bellows of the movable coil is of single-wall construction, thereby allowing it to approach the low temperatures of the venting helium gas. This cooled surface acts as a cryopump.

Vacuum System

The superconducting magnet system described in the preceding section is designed to fit into a vacuum tank that forms the outer canister of the superconducting magnet Dewar.

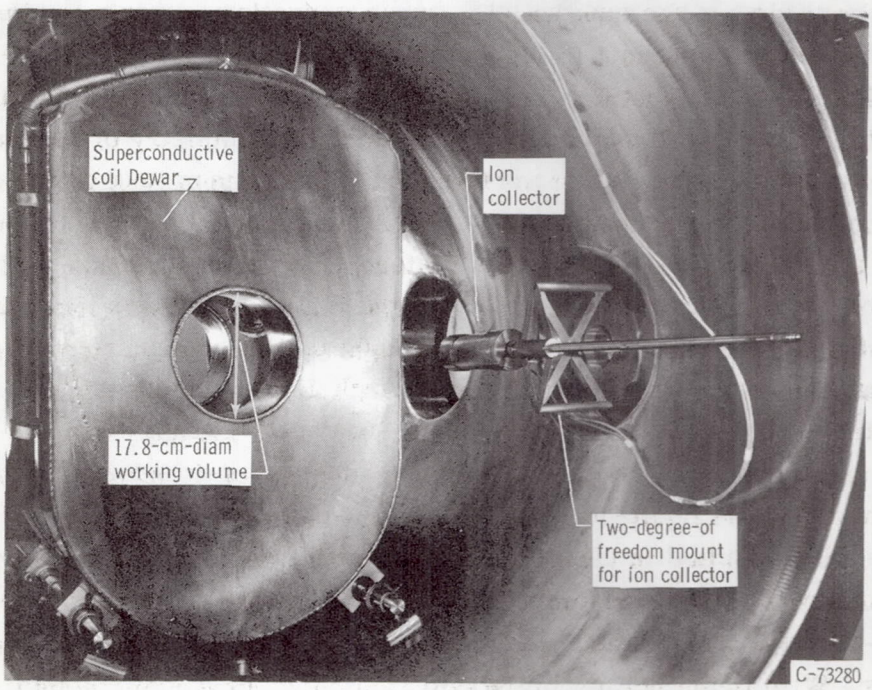

Figure 25. - End view of superconducting magnet assembly taken with end plate removed from tank.

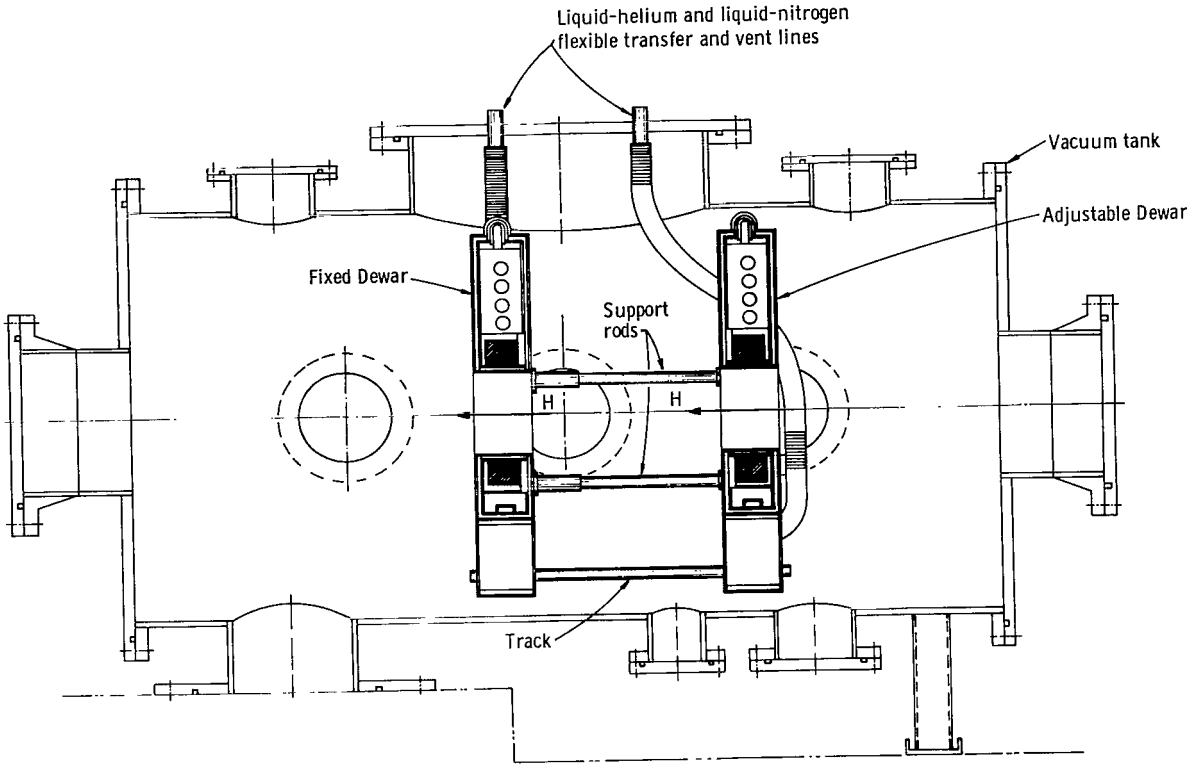

Figure 26. - Cutaway drawing of vacuum tank and coil Dewars.

A cross-sectional view of the tank with the superconducting magnets in place is shown in figure 26. The vacuum tank is 1 meter in diameter, 2 meters long, and fabricated of 0.95-inch-thick 304 nonmagnetic stainless steel. All bolts and exterior fittings on the tank are of stainless steel to avoid perturbing the axial symmetry of the magnetic field. All ports are sealed by single neoprene O-rings. The vacuum tank was designed with an unusually large number of access ports in order to exploit fully the excellent visual and instrumental access to the working volume afforded by the superconducting coils.

An air-lock system was attached to the right axial port, shown in figure 26, to reduce the number of times that the tank had to be brought up to atmospheric pressure. Among the probes that can be inserted through the air lock are a Langmuir probe, a Faraday cup, a hot-wire probe, and an emissive probe. A double Faraday cup and the ion source are mounted on sliding seals that permit the two-degree-of-freedom manipulation of both.

Cryopumping by the liquid-nitrogen and liquid-helium temperature surfaces exposed to the tank vacuum resulted in unexpectedly low tank pressures. The ultimate pressure of the vacuum tank with the coil assembly at room temperature is 2×10^{-6} torr. Cryopumping on the liquid-nitrogen temperature surfaces of the Dewars results in a pressure of 1.5×10^{-7} torr. With liquid helium in the coil assembly, cryopumping on the liquid-helium temperature surfaces reduces the tank pressure to below 3×10^{-8} torr.

APPENDIX C

COMPUTER PROGRAM FOR CALCULATION OF NONADIABATIC MOTION OF CHARGED PARTICLE IN MULTIPOLAR MAGNETIC BARRIER

by Paul Swigert

A computer program to integrate equations (18) to (20) was written in FORTRAN IV for the IBM 7094-7044 direct-couple system. This program integrated the three second-order differential equations, checked for different stopping conditions, and kept track of the number of particles at each stopping condition. The FORTRAN listings of the main program and related subroutines, flow charts for the main program (fig. 27) and the integration subroutine (fig. 28), and a step-by-step explanation of the main program are also presented.

The functions of other related subroutines are given as follows: Subroutine DIFF evaluates the differential equations for the integration subroutine. The three second-order differential equations were transformed into a set of six first-order equations so that the first-order Runge-Kutta method could be used. Subroutine ADI computes M_4 at each integration step and stores the largest and smallest over the range of integration so that equation (26) can be computed. The listing for subroutine BESI is not included because a program of this type is available at most computing laboratories. The purpose of this subroutine is to compute the Bessel functions I_0 and I_1. The argument of the CALL statement is an array dimensioned by three, the Bessel function argument is the first element of this array, and the functions I_0 and I_1 are returned in the second and third elements of the array, respectively.

Various methods were used to establish the accuracy of the complete program. During the preliminary running of the program, the differential equations were subjected to a time reversal. Time reversal had no effect on the results of the integration other than to produce the mirror image of the trajectory. It was desirable to include in the program a means of making the integration interval proportional to the radius of curvature of the trajectory, since otherwise the kinetic energy, which should remain constant, changed considerably over the range of integration. With the provision for halving and doubling the increment at certain times, the kinetic energy changed by less than 1 percent over the complete trajectory and was not allowed to vary by more than 0.005 percent for each integration step. Finally, the results of this program were checked against a similar program given in reference 1.

This program was used to investigate the trajectories of 101 520 particles. With the initial conditions given in table I these particles were divided into 5076 cases of 20 parti-

cles each. The average computer time for each case was 1.24 minutes with extreme running times of 0.2 minute and 3.5 minutes. The wide spread in computer times occurred because the calculation of an individual particle was stopped when it became nonadiabatic, that is, when M_4 varied by more than 5 percent along the trajectory.

Description of Flow Chart for Main Program

The numbers in this section refer to the flow chart box numbers and the statement numbers in the FORTRAN listing.

(1) The 20 initial conditions given in table I are read into the computer at this point. These input cards should be arranged as follows: The first card contains the number of particles in fixed point notation ending in card column 5. The following cards contain the initial velocities in floating-point notation. These initial conditions η', α', and $\alpha\theta'$ must end in card columns 10, 20, and 30, respectively. There must be one of these cards for each particle. (See sample data on the FORTRAN listing of the main program.)

(2) The other initial conditions for the differential equations, the test for the kinetic energy constant, and a check to indicate if the program is to stop computing when a particle becomes nonadiabatic, are read in. This information is contained on one card and determines the conditions for one case. KTR and N are fixed-point numbers and must end in card columns 5 and 10, respectively. The other data take 10 card columns each and are in floating-point notation. Many of these cards may be placed at the end of the deck to allow running consecutive cases. (See sample data.)

(3) The quantities that will remain constant for the 20 initial conditions are computed and the counter array is initialized.

(4) The initial conditions are set up for the differential equations, and the kinetic energy at these initial conditions is evaluated.

(5) The integration subroutine is called for initialization. This call does not advance the solution.

(6) The values of the differential equations are stored so that the increment of the independent variable may be halved if necessary.

(7) The integration subroutine is called to advance the solution one increment.

(8) The kinetic energy is computed for this new step.

(9) If the kinetic energy has not changed by more than 0.005 percent, step (11) is performed.

(10) The independent variable is backed up one increment, and a new point is computed by integrating with a halved increment using the previously stored values of the differential equations as initial conditions.

(11) If six or more points have been computed with one increment and the kinetic

energy of the last calculation did not change by more than 0.0005 percent, the process is continued and the increment is doubled. If the increment is more than 0.0005 percent, step (13) is performed.

(12) The increment is doubled.

(13) If any of the following stopping conditions have been met, step (14) is performed. If these conditions have not been met, step (6) is performed.

Stopping conditions:

(a) The particle became nonadiabatic and the proper test was read in.

(b) $\alpha \geq \pi$.

(c) $\eta \geq \pi$.

(d) $\eta \leq 0$, and at least 16 points have been computed.

(e) The kinetic energy has changed by more than 1 percent over the trajectory.

(f) More than 2500 points have been computed for one trajectory.

(g) The increment became less than 2^{-24}.

(14) At this point the program keeps track of the number of particles stopped by each of the preceding conditions.

(15) If there are more particles to process, step (4) is performed.

(16) The counters are normalized in this step.

(17) The output is printed, and more data are read into the computer for the next case.

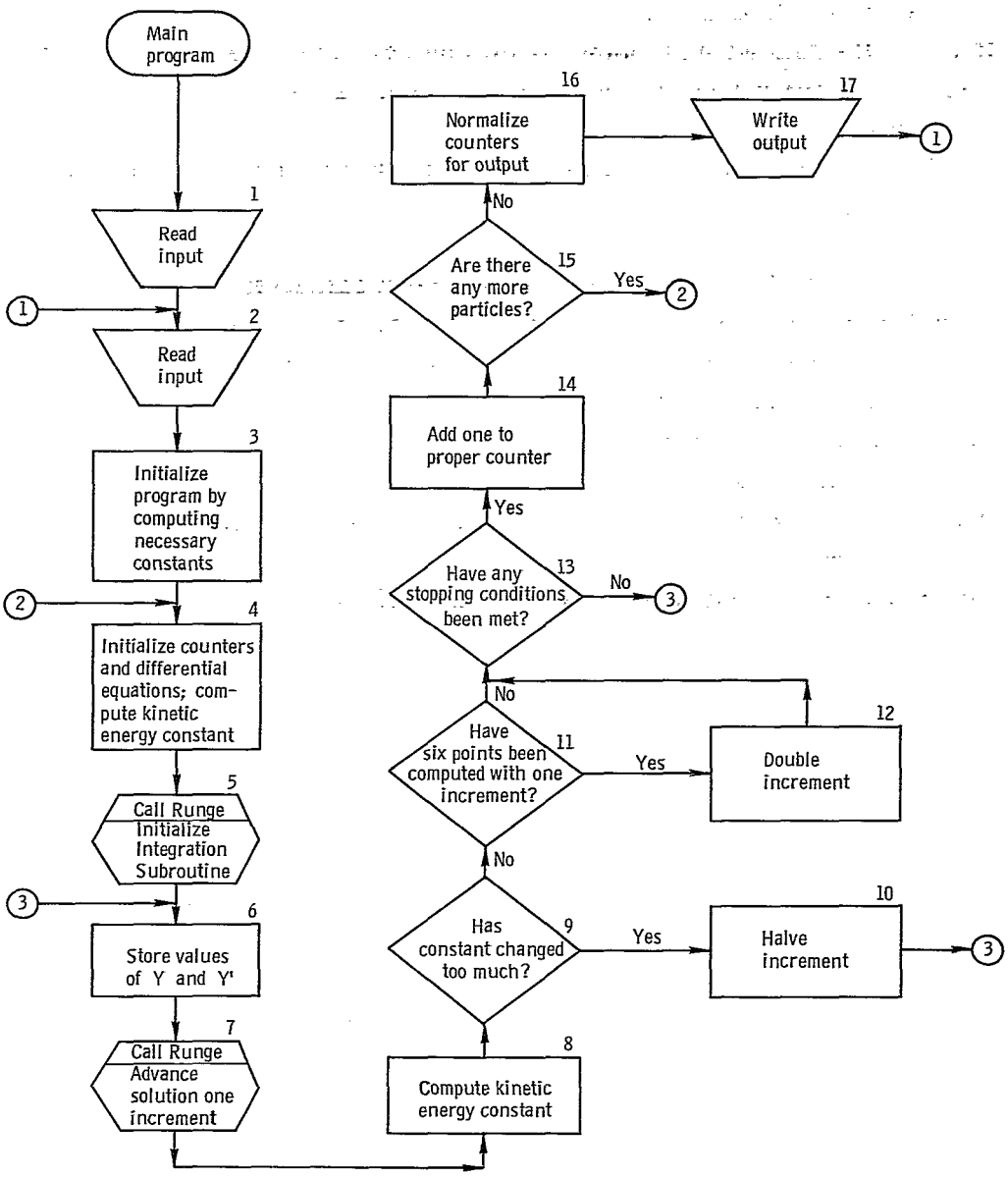

Figure 27. - Flow chart for Main program.

Main Program

```
C      NONADIABATIC MOTION OF A CHARGED PARTICLE IN A MULTIPOLAR
C      MAGNETIC BARRIER
       EXTERNAL DIFF
       COMMON N,RN,C12,C13,COETA,SIETA,CONTH,SINTH,ALFN1,Z
       COMMON /COM1/ N1,N2,V1,V2,V3,V4,V5,V6,V7
       DIMENSION ETAP(100),ALPHAP(100),THETAP(10 ),Z(3),Y(6),DY(6),K(8),
      *XK(8),YP(6),DYP(6)
     1 READ (5,501) NUM,(ETAP(I),ALPHAP(I),THETAP(I),I=1,NUM)
     2 READ (5,502) KTR,N,ALPHA,THETA,DELTA,RM,EPS,TEST,CHECK
C      NUM = NUMBER OF PARTICLES TO BE PROCESSED
C      ETAP = NONDIMENSIONAL AXIAL VELOCITY - ETA PRIME
C      ALPAHP = NONDIMENSIONAL RADIAL VELOCITY - ALPHA PRIME
C      THETAP = NONDIMENSIONAL ANGULAR VELOCITY - ALPHA*THETA PRIME
C      KTR = 0  THE PARTICLES ARE NOT STOPPED WHEN THEY BECOME NONADIABATIC
C            1  THE PARTICLES ARE STOPPED WHEN THEY BECOME NONADIABATIC
C      N = NUMBER OF PAIRS OF MULTIPOLAR CURRENTS
C      ALPHA = NONDIMENSIONAL RADIAL POSITION EQUATION 10
C      THETA = ANGULAR COORDINATE
C      DELTA = RADIAL MIRROR RATIO EQUATION 24
C      RM = MIRROR RATIO EQUATION 11
C      EPS = ADIABATIC PARAMETER EQUATION 3 - EPSILON
C      TEST = A TEST ON THE RELATIVE CHANGE OF THE KINETIC ENERGY CONSTANT
C             FROM ONE STEP TO THE NEXT
C      CHECK = A TEST ON THE ADIABATICY OF THE PARTICLES = M4(MAX)/M4(MIN)
       CALL TIME1(CL1)
       RNUM = NUM
     3 TEST1 = TEST/10.0
       RN = N
       N1 = N - 1
       N2 = 2*N1
       SCALE = 3.1415926*EPS
       Z(1) = ALPHA
       CALL BESI(Z)
       C13 = -(1.0-RM)/(Z(2)*(1.0+RM))
       C12 = DELTA*(C13+1.0)/(3.1415926**N1)
       V1 = 2.0*C13
       V2 = C13*C13
       V3 = C12*C12
       V4 = C12*V1
       V5 = 2.0*C12
       V6 = 2.0*V2
       V7 = 2.0*V3
       DO 31 J=1,8
    31 K(J) = 0
     4 DO 15 I=1,NUM
       XMH = 0.0
       XML = 1.0E+37
       KTR1 = 0
       KTR2 = 0
       KTR3 = 0
       KTR4 = 0
       H = 0.0078125
       X = 0.0
       Y(1) = ALPHAP(I)*SCALE
       Y(2) = THETAP(I)*SCALE/ALPHA
       Y(3) = ETAP(I)*SCALE
       Y(4) = ALPHA
       Y(5) = THETA
       Y(6) = 0.
       T0 = Y(3)**2 + Y(4)**2*Y(2)**2 + Y(1)**2
       T1 = T0
```

```
  5 CALL RUNGE(6,H,X,Y,DY,0,DIFF)
 51 DO 6 J=1,6
    DYP(J) = DY(J)
  6 YP(J) = Y(J)
  7 CALL RUNGE(6,H,X,Y,DY,1,DIFF)
  8 T2 = Y(3)**2 + Y(4)**2*Y(2)**2 + Y(1)**2
    A = ABS(T2/T1-1.0)
  9 IF(A.GT.TEST)  GO TO 10
 11 IF(A.LT.TEST1.AND.KTR3.GT.5)  GO TO 12
 13 KTR2 = KTR2 + 1
    KTR3 = KTR3 + 1
    T1 = T2
    IF(KTR4.EQ.0)  CALL ADI(Y,DY,XMH,XML)
    IF(XMH/XML.GE.CHECK)  KTR4 = 1
    IF(KTR4.EQ.1.AND.KTR.EQ.1)  GO TO 146
    IF(Y(4).GE.3.1415926)  GO TO 14
    IF(Y(6).GE.3.1415926)  GO TO 141
    IF(Y(6).LE.0.0.AND.KTR2.GE.16)  GO TO 142
    IF(ABS(T2/T0-1.0).GT.0.01)  GO TO 143
    IF(KTR2.GT.2500)  GO TO 144
    GO TO 51
 10 IF(KTR1.GT.17)  GO TO 145
    KTR1 = KTR1 + 1
    X = X-H
    H = H/2.0
    DO 101 J=1,6
    DY(J) = DYP(J)
101 Y(J) = YP(J)
    KTR3 = 0
    GO TO 7
 12 KTR1 = KTR1 - 1
    H = 2.0*H
    KTR3 = 0
    GO TO 13
 14 K(1) = K(1) + 1
    GO TO 147
141 K(2) = K(2) + 1
    GO TO 147
142 K(3) = K(3) + 1
    GO TO 147
143 K(4) = K(4) + 1
    GO TO 147
144 K(5) = K(5) + 1
    GO TO 147
145 K(6) = K(6) + 1
    GO TO 147
146 K(7) = K(7) + 1
    GO TO 15
147 IF(KTR4.EQ.0)  K(8) = K(8) + 1
 15 CONTINUE
    DO 16 J=1,8
    XK(J) = K(J)
 16 XK(J) = XK(J)/RNUM
    CALL TIME1(CL2)
    TIME = ABS(CL2-CL1)/3600.0
 17 WRITE (6,601) N,ALPHA,THETA,C12,C13,SCALE,TEST,CHECK,DELTA,RM,EPS,
   *(XK(J),J=1,8)
    WRITE (6,602) NUM,TIME
    GO TO 2
501 FORMAT (I5,/,(3E10.0))
502 FORMAT (2I5,7E10.0)
```

```
  601 FORMAT (1H1,/,1H4,2HN=,I2,2X,6HALPHA=,G12.5,2X,6HTHETA=,G12.5,2X,4
     *HC12=,G12.5,2X,4HC13=,G12.5,2X,6HSCALE=,G12.5,2X,5HTEST=,G12.5,/,
     *7H CHECK=,G12.5,2X,6HDELTA=,G12.5,2X,3HRM=,G12.5,8HEPSILON=,G12.5,
     *            /,1HK,F7.4,56H  OF THE PARTICLES WERE STOPPED AT ALPHA
     * .GE. 3.14159265,/,1HK,F7.4,54H  OF THE PARTICLES WERE STOPPED AT
     *ETA .GE. 3.14159265,/,1HK,F7.4,47H  OF THE PARTICLES WERE STOPPED
     *AT ETA .LE. 0.0,/,1HK,F7.4,53H  OF THE PARTICLES WERE STOPPED BECA
     *USE OF DRIFT IN T,/,1HK,F7.4,65H  OF THE PARTICLES WERE STOPPED BE
     *CAUSE 2500 POINTS WERE COMPUTED,/,1HK,F7.4,75H  OF THE PARTICLES W
     *ERE STOPPED BECAUSE THE INCREMENT WAS LESS THAN 1/2**24,/,1HK,F7.4
     *,64H  OF THE PARTICLES WERE STOPPED BECAUSE THEY BECAME NONADIABAT
     *IC,/,1HK,F7.4
     *,33H  OF THE PARTICLES WERE ADIABATIC)
  602 FORMAT (15HKTHIS RUN USED ,I2,31H POINTS WITH AN ELAPSED TIME OF,F
     *5.2,5H MIN.)
      END
```

Sample Data

```
$DATA
  20
    0.00 0.7071068 0.7071068
    0.05 0.7062223-0.7062223
    0.10 0.7035624 0.7035624
    0.15 0.6991008-0.6991008
    0.20 0.6928203 0.6928203
    0.25 0.6846532-0.6846532
    0.30 0.6745369 0.6745369
    0.35 0.6623821-0.6623821
    0.40 0.6480741 0.6480741
    0.45 0.6314665-0.6314665
    0.50 0.6123724 0.6123724
    0.55 0.5905506-0.5905506
    0.60 0.5656854 0.5656854
    0.65 0.5373546-0.5373546
    0.70 0.5049752 0.5049752
    0.75 0.4677072-0.4677072
    0.80 0.4242641 0.4242641
    0.85 0.3724916-0.3724916
    0.90 0.3082207 0.3082207
    0.95 0.2207940-0.2207940
  1    2      0.50    0.7854      1.00      .15       .010     5.0E-5     1.050
  1    2      0.50    0.7854      1.00      .20       .010     5.0E-5     1.050
  1    2      0.50    0.7854      1.00      .30       .010     5.0E-5     1.050
```

```
      SUBROUTINE DIFF(T,Y,DY)
C     THIS SUBROUTINE EVALUATES THE SIX FIRST ORDER DIFFERENTIAL
C     EQUATIONS FOR SUBROUTINE RUNGE.
      DIMENSION Y(1),DY(1),Z(3)
      COMMON N,RN,C12,C13,COETA,SIETA,CONTH,SINTH,ALFN1,Z
      COETA = COS(Y(6))
      SIETA = SIN(Y(6))
      V = RN*Y(5)
      CONTH = COS(V)
      SINTH = SIN(V)
      Z(1) = Y(4)
      CALL BESI(Z)
      ALFN = Y(4)**N
      ALFN1 = ALFN/Y(4)
      V1 = Y(4)*Y(2)
      V2 = C13*V1
      V3 = C12*Y(3)*ALFN1
      V4 = COETA*Z(2)
      V5 = SIETA*Z(3)
      DY(1) = Y(2)*V1+V3*SINTH+V1+V2*V4
      DY(2) =(-2.0*Y(2)*Y(1)-Y(1)+C13*Y(3)*V5-C13*Y(1)*V4+V3*CONTH)/Y(4)
      DY(3) = -C12*Y(1)*ALFN1*SINTH-C12*ALFN*Y(2)*CONTH-V2*V5
      DY(4) = Y(1)
      DY(5) = Y(2)
      DY(6) = Y(3)
      RETURN
      END
```

```
      SUBROUTINE ADI(Y,DY,XMH,XML)
C     THIS SUBROUTINE COMPUTES M4 AND STORES THE EXTREME VALUES, I.E.
C     M4(HIGH), M4(LOW).
      COMMON N,RN,C12,C13,COETA,SIETA,CONTH,SINTH,V9,Z
      COMMON /COM1/ N1,N2,V1,V2,V3,V4,V5,V6,V7
      DIMENSION Y(1),DY(1),Z(3)
      X0 = V1*COETA*Z(2)
      X1 = V2*SIETA**2*Z(3)**2
      X2 = V2*COETA**2*Z(2)**2
      V8 = V9**2
      X3 = V3*V8
      X4 = V4*V9*SIETA*CONTH*Z(3)
      X5 = V5*V9*SINTH
      Q = X0*C12*V9
      X6 = Q*SINTH
      X7 = Q*CONTH
      X8 = V1*SIETA*Z(3)
      X9 = V6*SIETA*COETA*Z(2)*Z(3)
      X10 = V5*V9*CONTH
      X11 = V7*V8*CONTH*SINTH+V4*V9*SIETA*SINTH*Z(3)
      B = 1.0+X0+X1+X2+X3+X4
      B = SQRT(B)*B
      VB = (Y(4)*Y(2))**2*(1.0+X2+X0+X3*CONTH**2+X1+X4) + Y(3)**2*(X3+X1
     *+X4) + Y(1)**2*(1.0+X2+X0+X3*SINTH**2) + Y(3)*Y(4)*Y(2)*(X5+X6) -
     * Y(1)*Y(3)*(X7+X8+X9+X10) + Y(1)*Y(4)*Y(2)*X11
      H = VB/B
      IF(H.GT.XMH)  XMH = H
      IF(H.LT.XML)  XML = H
      RETURN
      END
```

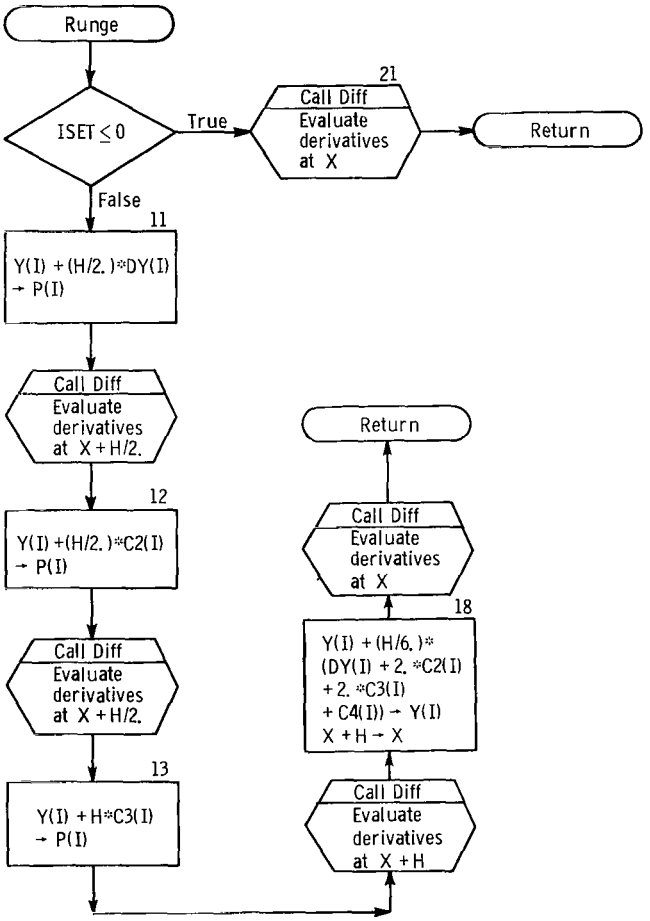

Figure 28. - Flow chart for Integration subroutine.

```
      SUBROUTINE RUNGE(N,H,X,Y,DY,ISET,F)
C     SUBROUTINE TO INTEGRATE N FIRST ORDER DIFFERENTIAL EQUATIONS.
C          N = NUMBER OF EQUATIONS TO BE INTEGRATED.
C          H = INCREMENT OF THE INDEPENDENT VARIABLE.
C          X = INDEPENDENT VARIABLE.
C          Y = ARRAY OF N DEPENDENT VARIABLES.
C          DY = ARRAY OF N DERIVITAVES OF THE DEPENDENT VARIABLES.
C          ISET = 0  FOR INITIALIZATION
C               = 1  TO ADVANCE THE SOLUTION ONE INCREMENT.
C          F = NAME OF THE SUBROUTINE PROVIDED TO EVALUATE THE
C              N DIFFERENTIAL EQUATIONS.  THIS NAME MUST APPEAR IN
C              AN EXTERNAL CARD OF THE CALLING PROGRAM.
      DIMENSION Y(1),DY(1),P(24),C2(24),C3(24),C4(24)
      IF(ISET) 21,21,1
   21 CALL F (X,Y,DY)
      GO TO 10
    1 DO 11  I=1,N
   11 P(I) = Y(I) + (H/2.)*DY(I)
      CALL F(X+H/2.,P,C2)
      DO 12  I=1,N
   12 P(I) = Y(I)+(H/2.)*C2(I)
      CALL F(X+H/2.,P,C3)
      DO 13  I=1,N
   13 P(I) = Y(I)+H*C3(I)
      CALL F(X+H,P,C4)
      DO 18  I=1,N
   18 Y(I)  = Y(I)+(H/6.)*(DY(I)+2.*C2(I)+2.*C3(I)+C4(I))
      X = X+H
      CALL F(X,Y,DY)
   10 RETURN
      END
```

REFERENCES

1. Roth, J. Reece: Nonadiabatic Motion of a Charged Particle in an Axisymmetric Magnetic Barrier. Phys. Fluids, vol. 7, no. 4, Apr. 1964, pp. 536-543.

2. Roth, John Reece: On the Nonadiabatic Motion of a Charged Particle in an Axisymmetric Magnetic Barrier. Ph.D. Thesis, Cornell Univ., 1963.

3. Glasstone, Samuel; and Lovberg, Ralph H.: Controlled Thermonuclear Reactions, an Introduction to Theory and Experiment. D. Van Nostrand Co., Inc., 1960, p. 344.

4. Garren, A.; Riddell, R.J.; Smith, L.; Bing, G.; Henrich, L.R.; Northrop, T.G.; and Roberts, J.E.: Individual Particle Motion and the Effect of Scattering in an Axially Symmetric Magnetic Field. Theoretical and Experimental Aspects of Controlled Nuclear Fusion. Vol. 31 of the Proceedings of the Second United Nations International Conference on the Peaceful Uses of Atomic Energy, United Nations (Geneva), 1958, pp. 65-71.

5. Kuo, L.G.; Murphy, E.G.; Petravic, M.; and Sweetman, D.R.: Remarks on the Finite Larmor Radius Stabilization Theory for Mirror Machines. J. Nucl. Energy, Pt. C, vol. 6, 1964, pp. 505-510.

6. Harris, E.G.: Plasma Instabilities Associated with Anisotropic Velocity Distributions. J. Nucl. Energy, Pt. C, vol. 2, 1961, pp. 138-145.

7. Grad, Harold; and Van Norton, Roger: Nonadiabatic Orbits in a Cusped Magnetic Field. Nucl. Fusion, Suppl., pt. 1, 1962, pp. 61-65.

8. Yoshikawa, S.: Nonadiabatic Motion of a Charged Particle in a Mirror Magnetic Field. Quarterly Progress Rept. No. 55, Research Lab. of Electronics, Massachusetts Inst. of Tech., Oct. 1959, pp. 27-30.

9. Gibson, G.; Jordan, W.C.; and Lauer, E.J.: Particle Behavior in Static, Axially Symmetric, and Magnetic Mirror and Cusp Geometries. Phys. Fluids, vol. 6, no. 1, Jan. 1963, pp. 116-133.

10. Rodionov, S.N.: An Experimental Test of the Behaviour of Charged Particles in an Adiabatic Trap. J. Nucl. Energy, Pt. C., vol. 1, no. 4, July 1960, pp. 247-252.

11. Dandl, R.A.; England, A.C.; Ard, W.B.; Eason, H.O.; Becker, M.C.; and Haas, G.M.: Properties of a High-Beta Plasma Produced by Electron-Cyclotron Heating. Nucl. Fusion, vol. 4, no. 4, 1964, pp. 344-353.

12. Meyerand, Russell G., Jr.; and Brown, Sanborn C.: High Current Ion Source. Rev. Sci. Instr., vol. 30, no. 2, Feb. 1959, pp. 110-111.

13. Brevnov, N. N.; and Tomashchuk, Yu. F.: The Effect of Local Perturbations of a Magnetic Field on the Trapping of Particles in an Adiabatic Magnetic Mirror Machine. J. Nucl. Energy, Pt. C, vol. 6, 1964, pp. 161-171.

TABLE I. - VELOCITY INITIAL CONDITIONS OF TWENTY PARTICLES USED TO DETERMINE FRACTION OF PARTICLES ADIABATIC

Dimensionless axial velocity, η'	Dimensionless radial velocity, α'	Dimensionless azimuthal velocity, α_θ'
0	0.7071068	0.7071068
.05	.7062223	-.7062223
.10	.7035624	.7035624
.15	.6991008	-.6991008
.20	.6928203	.6928203
.25	.6846532	-.6846532
.30	.6745369	.6745369
.35	.6623821	-.6623821
.40	.6480741	.6480741
.45	.6314665	-.6314665
.50	.6123724	.6123724
.55	.5905506	-.5905506
.60	.5656854	.5656854
.65	.5373546	-.5373546
.70	.5049752	.5049752
.75	.4677072	-.4677072
.80	.4242641	.4242641
.85	.3724916	-.3724916
.90	.3082207	.3082207
.95	.2207940	-.2207940

TABLE II. - CONSTANTS FOR RELATION $\epsilon_o = C_4(1 - F)^{E_1} + C_5(1 - F)^{E_2}$

Number of pairs of multipolar currents, n	Radial mirror ratio, δ	Nondimensional radius, α							
		0.05	0.25	0.50	0.75	1.00	1.50	2.00	2.50
					C_4				
2	0	0.1174	0.235	0.385	------	0.146	0.1659	0.1676	0.1490
	.25	.1097	.1959	.1591	0.1707	.152	.1570	.1730	.1280
	.50	.1600	.1623	.370	.1491	.120	.1695	.198	.0706
	.75	.1483	.086	.1264	.1179	.1331	.5588	.0973	.1998
	1.00	.1580	3.00	.1168	.1850	.2069	.320	------	------
	1.50	------	------	------	------	------	------	------	------
3	0.25	0.1695	0.222	0.210	0.1812	0.1501	0.1534	0.1187	0.1535
	.50	.1735	.233	.1466	.1460	.1386	.1499	.166	.115
	.75	.1680	.1625	.1505	.1319	.1198	.1352	.1150	------
	1.00	.1690	.1450	.1521	.1281	.1436	.2009	------	------
	1.50	.1597	.185	.1337	.1306	.1408	------	------	------
					C_5				
2	0	0	0.620	0.203	------	0.068	0	0	0
	.25	.0519	.2295	.3154	0.3417	.120	.125	.220	.1070
	.50	0	.5918	.157	.1406	.074	0	0	.1751
	.75	.3688	.800	1.5061	.2986	.5465	.1285	.1809	0
	1.00	.2261	.102	.7719	.088	0	.144	------	------
	1.50	------	------	------	------	------	------	------	------
3	0.25	0	0.550	0.190	0	0	0	0.0595	0.0463
	.50	0	1.30	.2770	.1796	.1464	.1143	0	.450
	.75	0	1.30	.2632	.1887	.0753	.2182	.350	------
	1.00	0	.485	.3377	.2224	.3654	.0915	------	------
	1.50	.0304	.335	.3961	.409	.3794	------	------	------

TABLE II. - Concluded. CONSTANTS FOR RELATION $\epsilon_o = C_4(1 - F)^{E_1} + C_5(1 - F)^{E_2}$

Number of pairs of multipolar currents, n	Radial mirror ratio, δ	Nondimensional radius, α							
		0.05	0.25	0.50	0.75	1.00	1.50	2.00	2.50
					E_1				
2	0	0.0256	0.455	7.22	-------	0.180	0.2259	0.3136	0.1713
	.25	-.0286	.1986	.2079	0.3466	.430	.420	.555	.260
	.50	.5574	.5494	9.25	.5635	.500	.8291	.980	-.1307
	.75	.7987	.310	.607	.5073	.6537	-.1158	.1600	.5973
	1.00	1.2317	15.50	.7322	4.70	1.7614	11.60	-------	-------
	1.50	--------	-------	--------	-------	-------	-------	-------	-------
3	0.25	0.02632	0.134	0.195	0.2113	0.3030	0.3665	0.3692	0.6661
	.50	.0731	.260	.03252	.2226	.3923	.6796	1.00	.520
	.75	.05766	0	.1764	.3080	.4169	.9117	.700	-------
	1.00	.0539	0	.3032	.4366	.7894	7.7503	-------	-------
	1.50	.04686	.290	.4211	.7515	1.1109	-------	-------	-------
					E_2				
2	0	0	4.86	0.090	-------	6.87	0	0	0
	.25	.6487	6.741	5.122	15.40	11.20	18.20	20.60	5.25
	.50	0	10.437	.630	7.4054	5.44	0	0	3.0405
	.75	18.753	6.380	20.184	12.590	22.146	2.641	6.2142	0
	1.00	11.588	.620	15.827	.4550	0	1.45	-------	-------
	1.50	--------	-------	-------	-------	-------	-------	-------	-------
3	0.25	0	4.160	4.56	0	0	0	2.487	7.077
	.50	0	7.30	4.1816	9.5807	11.093	13.632	0	12.80
	.75	0	5.40	6.3970	7.4901	5.3557	17.098	12.00	-------
	1.00	0	3.38	10.167	10.340	24.714	.5127	-------	-------
	1.50	8.1517	3.92	7.8666	14.780	16.154	-------	-------	-------

TABLE III. - CONSTANTS FOR RELATIONS

$A_o = A_{oA}(1 - F)^{E_3}$ AND $K = K_o(1 - F)^{E_4}$

Number of pairs of multipolar currents, n	Radial mirror ratio, δ	A_{oA}	E_3	K_o	E_4
2	0	0.3441	0.1780	-0.2531	-0.0796
	.25	.3411	.1577	-.2692	-.1136
	.50	.3291	.0491	-.3023	-.1391
	.75	.3222	.047	-.3216	-.2192
	1.00	.3130	-.2147	-.2750	-.155
	1.50	------	------	------	------
3	0.25	0.3611	0.1983	-0.2405	-0.1259
	.50	.3419	.080	-.250	0
	.75	.350	.067	-.250	.84
	1.00	.3552	.0148	-.252	.280
	1.50	.385	.0310	-.250	.432

TABLE IV. - DATA RELEVANT TO ADIABATICITY FROM PRIOR EXPERIMENTS

Source	Axial distance between B_{min} and B_{max}, z_o, m	Minimum magnetic field strength on axis, B_{min}, W/m^2	Mirror ratio, $R_m \equiv \frac{B_{min}}{B_{max}}$	Charge species	Particle energy, V, eV	Plasma radius, r_p, m	Reduced plasma radius, $\alpha = \frac{\pi r_p}{z_o}$	Adiabatic parameter, $\epsilon \equiv \frac{\langle R_\ell \rangle}{z_o}$	Plotted point
Ref. 11 and England	0.254	0.260	0.550	Electron	8×10^4	0 to 0.10	≤ 1.24	0.0102	▲
	.254	.260	.550		1×10^6	0.05 to 0.15	$0.62 \leq \alpha \leq 1.86$	.0375	△
	.254	.260	.550		4×10^6	0.05 to 0.15	$0.62 \leq \alpha \leq 1.86$	.0750	△
	.457	.220	.324		1.2×10^5	0 to 0.20	≤ 1.37	.0057	▲
	.457	.220	.324		1×10^6	0.10 to 0.30	$0.69 \leq \alpha \leq 2.06$	.0164	△
	.457	.220	.324		4×10^6	0.10 to 0.30	$0.69 \leq \alpha \leq 2.06$	.0328	△
Alexeff	0.075	0.150	0.333	Electron	$\approx 1\times10^5$	0 to 0.03	≤ 1.25	0.0475	◣
Ref. 10	0.085	0.0300	0.200	Positron	$\approx 1.5\times10^3$	$\approx$0.0195	$\leq$0.72	0.017	■
		.0360	.200					.014	■
		.029	.200					.0176	□
		.005	.200					.102	□
		.009	.025					.0075	□
		.029	.073					.0071	□
		.029	.073					.0071	■
		.043	.108					.0069	■
		.021	.070					.0095	□
		.026	.087					.0094	□, ■
		.040	.133					.0090	■
Ref. 9	0.405	0.173	0.560	Positron	5×10^5	-------	$\leq$0.57	0.0244	●
		.130			5	-------		.0325	●
		.065			5	-------		.065	○
		.0578			5	-------		.073	○
		.173			1×10^6	-------		.0345	●
		.130				-------		.046	●
		.065				-------		.092	○
		.0578				-------		.103	○
		.0506				-------		.118	○
		.0939				-------		.064	●
	.410	.065	.59		5×10^5	-------		.066	○
	.410	.130	.59		5	-------		.033	●
	.625	.059	.286		5	-------	$\leq$0.38	.0288	○

TABLE IV. - Concluded. DATA RELEVANT TO ADIABATICITY FROM PRIOR EXPERIMENTS

Source	Axial distance between B_{min} and B_{max}, z_o, m	Minimum magnetic field strength on axis, B_{min}, W/m^2	Mirror ratio, $R_m \equiv \frac{B_{min}}{B_{max}}$	Charge species	Particle energy, V, eV	Plasma radius, r_p, m	Reduced plasma radius, $\alpha = \frac{\pi r_p}{z_o}$	Adiabatic parameter, $\epsilon \equiv \frac{\langle R_\ell \rangle}{z_o}$	Plotted point
Ref. 9	0.625	0.079	0.286	Electron	5×10^5	------	$\leq$0.38	0.0214	○
	.410	.065	.59		1×10^6	------	$\leq$0.57	.0935	○
	.410	.130	.59		1	------	$\leq$0.57	.0468	●
	.625	.059	.286		1	------	$\leq$0.38	.0406	○
	.535	.093	.91		5×10^5	------	$\leq$0.89	.0458	●
	.535	.186	.91			------	$\leq$0.89	.0229	●
	.535	.280	.91			------	$\leq$0.89	.0151	●
	.810	.057	.59			------	$\leq$0.59	.038	●
	.810	.096	.59			------	$\leq$0.59	.0226	●
	.810	.130	.59			------	$\leq$0.59	.0167	●
	.810	.172	.59			------	$\leq$0.59	.0126	●
	1.25	.053	.27			------	$\leq$0.38	.0152	○
	1.25	.072	.27			------	$\leq$0.38	.0112	○
	.535	.186	.91		1×10^6	------	$\leq$0.89	.0324	●
	.535	.280	.91			------	$\leq$0.89	.0214	●
	.810	.057	.59			------	$\leq$0.59	.054	●
	.810	.096	.59			------	$\leq$0.59	.022	●
	.810	.130	.59			------	$\leq$0.59	.0237	●
	.810	.172	.59			------	$\leq$0.59	.0179	●
	1.25	.053	.27			------	$\leq$0.38	.0216	○
	1.25	.072	.27			------	$\leq$0.38	.0159	○
	.405	.130	.56			------	$\leq$0.57	.0326	●
	.405	.130	.56			------	$\geq$1.14	.0326	○
Refs. 1 and 2	0.196	0.1245	0.465	Helium ion	5.7	------	$\leq$0.10	0.028	◇
	.210	.209	.262		9.4	------		.021	◇
	.198	.256	.188		10.0	------		.018	◇
	.214	.223	.256		11.0	------		.020	◇
	.208	.24	.238		10.0	------		.018	◇
	.196	.18	.27		4.4	------		.017	◇
	.23	.34	.214		24.0	------		.018	◇
	.13	.20	.404		18.0	------		.049	◇
	.24	.25	.165		10.5	------		.016	◇
	.22	.41	.31		14	------		.012	◇
	.24	.27	.20		23	------		.021	◇
	.25	.34	.16		21	------		.016	◇
	.17	.28	.28		30	------		.033	◇
	.20	.29	.34		23	------		.024	◇
	.20	.26	.38		24	------		.027	◇
	.14	.18	.46		17	------		.046	◇

TABLE V. - RAW EXPERIMENTAL DATA

Nondimensional radius, α	Axial distance between B_{min} and B_{max}, z_o, m	Average magnetic field, B_{av}, W/m^2	Charge species	Critical deuteron energy, V, eV	Adiabatic parameter, ϵ	Mirror ratio, R_m	Run
0.05	0.127	1.59	Singly charged helium ions	5200	0.100	0.63	27
	.127	1.59	↓	4900	.099	.63	28
	.127	1.59		5500	.104	.63	29
	.109	1.22		5200	.156	.73	51
	.109	1.22		5300	.158	.73	52
	.109	1.22		5300	.158	.73	53
	.114	.92		3000	.129	.70	69
	.114	.92		3100	.132	.70	70
	.114	.92		3300	.135	.70	71
	.117	1.51		7000	.136	.68	141
	.117	1.51		5600	.122	.68	142
	.117	1.51		5900	.125	.68	143
	.117	1.51		5600	.122	.68	144
	.102	.89		3700	.193	.78	149
	.102	.89		4300	.208	.78	150
	.102	.89		4200	.206	.78	151
	.084	.94		3900	.229	.87	189
	.084	.94		4100	.234	.87	190
	.084	.94		4100	.234	.87	191
	.059	.96		3850	.321	.95	202
	.059	.96		3950	.325	.95	203
	.059	.96		4000	.327	.95	204
	.061	1.89	Singly charged neon ions	2300	.271	.94	225
	.061	1.89	Singly charged neon ions	2500	.282	.94	226
	.133	.029	Electrons	6800	.072	.56	228
	↓	.029	↓	6600	.071	.56	229
		.029		7100	.074	.56	230
		.038		7500	.059	.52	246
		.038		7200	.058	.52	247
		.038		7500	.059	.52	248
	.146	.051		7700	.410	.43	264

TABLE V. - Continued. RAW EXPERIMENTAL DATA

Nondimensional radius, α	Axial distance between B_{min} and B_{max}, z_o, m	Average magnetic field, B_{av}, W/m^2	Charge species	Critical deuteron energy, V, eV	Adiabatic parameter, ϵ	Mirror ratio, R_m	Run
0.05	0.146	0.051	Electrons	7600	0.040	0.43	265
	.146	.051		7500	.040	.43	266
	.191	.0735		5000	.017	.32	281
	.191	.0735		4900	.017	.32	282
	.191	.0735		4900	.017	.32	283
	.165	.0620		5800	.025	.41	305
	.178	.059		3400	.019	.35	309
	.241	.168		2200	.0039	.175	319
	.241	.168		2000	.0037	.175	320
	.241	.168		2300	.0040	.175	321
	.203	.075		2700	.012	.26	328
	.203	.075		2400	.011	.26	329
	.203	.075		2600	.0115	.26	330
	.190	.089		4900	.014	.28	336
	.190	.089		5000	.014	.28	337
	.190	.089		5000	.014	.28	338
	.210	.125		4200	.0084	.23	348
	.210	.125		4600	.0087	.23	349
	.210	.125		4000	.0082	.23	350
0.25	0.127	1.59	Singly charged helium ions	5700	0.106	0.63	30
	.127	1.59		5400	.103	.63	31
	.127	1.59		5600	.105	.63	32
	.109	1.22		5800	.164	.73	54
	.109	1.22		5900	.167	.73	55
	.109	1.22		5900	.167	.73	56
	.114	.92		3100	.131	.70	72
	.114	.92		3400	.137	.70	73
	.114	.92		3600	.140	.70	74
	.117	1.51		5000	.115	.68	125
	.117	1.51		5100	.116	.68	126
	.117	1.51		4900	.114	.68	127
	.102	.90		4000	.200	.78	152
	.102	.90		4300	.210	.78	153
	.102	.90		4000	.20	.78	154

TABLE V. - Continued. RAW EXPERIMENTAL DATA

Nondimensional radius, α	Axial distance between B_{min} and B_{max}, z_o, m	Average magnetic field, B_{av}, W/m^2	Charge species	Critical deuteron energy, V, eV	Adiabatic parameter, ϵ	Mirror ratio, R_m	Run
0.25	0.084	0.940	Singly charged helium ions	4400	0.244	0.87	192
	.084	.940		4500	.245	.87	193
	.084	.940		4600	.249	.87	194
	.059	.955		3700	.31	.95	205
	.059	.955		3750	.32	.95	206
	.059	.955		4000	.33	.95	207
	.133	.029	Electrons	5200	.063	.56	231
		.029		5100	.063	.56	232
		.029		5200	.063	.56	233
		.029		5700	.066	.56	234
		.038		6700	.056	.515	249
		.038		6400	.054	.515	250
		.038		6300	.054	.515	251
	.146	.051		7400	.039	.43	267
	.146	.051		7400	.039	.43	268
	.146	.051		7800	.041	.43	269
	.191	.074		4900	.017	.32	284
	.191	.074		4100	.015	.32	285
	.191	.074		4500	.016	.32	286
	.178	.059		3800	.020	.35	310
	.178	.059		3800	.020	.35	311
	.178	.059		3500	.019	.35	312
	.241	.168		2000	.0037	.175	322
	.241	.168		2200	.0039	.175	323
	.241	.168		1600	.0033	.175	324
	.203	.075		2200	.0105	.26	331
	.203	.075		1900	.0097	.26	332
	.190	.089		3900	.012	.28	339
	.190	.089		4200	.013	.28	340
	.190	.089		4100	.013	.28	341
	.210	.125		3400	.076	.23	351
	.210	.125		3500	.076	.23	352
	.210	.125		3400	.075	.23	353

TABLE V. - Continued. RAW EXPERIMENTAL DATA

Nondimensional radius, α	Axial distance between B_{min} and B_{max}, z_o, m	Average magnetic field, B_{av}, W/m^2	Charge species	Critical deuteron energy, V, eV	Adiabatic parameter, ϵ	Mirror ratio, R_m	Run
0.50	0.117	1.51	Singly charged helium ions	5600	0.122	0.68	128
	.117	1.51		5500	.121	.68	129
	.117	1.51		5900	.125	.68	130
	.102	.900		4100	.204	.78	155
	.102	.900		4100	.204	.78	156
	.102	.900		4000	.20	.78	157
	.084	.94		4600	.25	.87	195
	.084	.94		4650	.25	.87	196
	.084	.94		4700	.25	.87	197
	.059	.96		4000	.33	.95	208
	.059	.96		4350	.34	.95	209
	.059	.96		4100	.33	.95	210
	.133	.029	Electrons	4600	.060	.56	235
		.029		4000	.056	.56	236
		.029		4200	.057	.56	237
		.038		6100	.053	.52	252
		.038		6000	.053	.52	253
		.038		6300	.054	.52	254
	.146	.051		7300	.039	.43	270
	.146	.051		6200	.036	.43	271
	.146	.051		6300	.037	.43	272
	.191	.074		3800	.015	.32	287
	.191	.074		3200	.014	.32	288
	.191	.0735		3200	.014	.32	289
	.241	.168		1600	.0033	.175	325
	.241	.168		1600	.0033	.175	326
	.241	.168		1500	.0032	.175	327
	.203	.0745		3200	.0126	.26	333
	.203	.0745		1900	.0097	.26	334
	.203	.0745		2000	.010	.26	335
	.190	.089		3600	.012	.28	342
	.190	.089		3400	.0116	.28	343
	.190	.089		3500	.0117	.28	344
	.210	.125		3500	.0077	.23	354
	.210	.125		3400	.0075	.23	355

TABLE V. - Continued. RAW EXPERIMENTAL DATA

Nondimensional radius, α	Axial distance between B_{min} and B_{max}, z_o m	Average magnetic field, B_{av}, W/m^2	Charge species	Critical deuteron energy, V, eV	Adiabatic parameter, ϵ	Mirror ratio, R_m	Run
0.75	0.127	1.59	Singly charged helium ions	2100	0.064	0.63	33
	.127	1.59		2500	.070	.63	34
	.127	1.59		2700	.073	.63	35
	.109	1.22		3700	.132	.73	66
	.109	1.22		3800	.134	.73	67
	.109	1.22		4100	.138	.73	68
	.114	.92		3700	.143	.70	75
	.114	.92		3100	.131	.70	76
	.117	1.51		6800	.134	.68	131
	.117	1.51		7200	.138	.68	132
	.117	1.51		8200	.147	.68	133
	.102	.896		4400	.210	.78	158
	.102	.896		3500	.190	.78	159
	.102	.896		3600	.190	.78	160
	.084	.940		4650	.250	.87	198
	.084	.940		4750	.252	.87	199
	.084	.940		4700	.251	.87	200
	.059	.955		4000	.326	.95	211
	.059	.955		3650	.312	.95	212
	.059	.955		3750	.317	.95	213
	.133	.029	Electrons	3600	.053	.56	238
		.029		4600	.059	.56	239
		.038		6000	.053	.515	255
		.038		6000	.053	.515	256
		.038		6400	.054	.515	257
	.146	.051		6200	.035	.432	273
	.146	.051		6600	.037	.432	274
	.152	.033		3000	.018	.350	313
	.152	.033		2700	.017	.350	314
	.152	.033		3100	.018	.350	315
	.190	.089		2900	.011	.284	345
	.190	.089		2900	.011	.284	346
	.190	.089		2800	.0105	.284	347

TABLE V. - Continued. RAW EXPERIMENTAL DATA

Nondimensional radius, α	Axial distance between B_{min} and B_{max}, z_o m	Average magnetic field, B_{av}, W/m^2	Charge species	Critical deuteron energy, V, eV	Adiabatic parameter, ϵ	Mirror ratio, R_m	Run
1.00	0.117	1.51	Singly charged helium ions	5200	0.118	0.68	135
	.117	1.51	↓	5100	.116	.68	136
	.117	1.51		4900	.114	.68	137
	.102	.900		2300	.153	.78	161
	.102	.900		2400	.156	.78	162
	.102	.900		3100	.177	.78	163
	.102	.900		3400	.185	.78	164
	.084	.94		4200	.238	.87	201
	.059	.96		3850	.32	.95	214
	.059	.96		3900	.32	.95	215
	.059	.96		3950	.33	.95	216
	.133	.029	Electrons	4200	.057	.56	240
	↓	.029	↓	4400	.058	.56	241
		.029		4600	.060	.56	242
		.038		4800	.047	.52	258
		.038		4600	.046	.52	259
		.038		4400	.045	.52	260
	.146	.051		5100	.033	.43	275
	.146	.051		5200	.033	.43	276
	.146	.051		5200	.033	.43	277
	.178	.059		2100	.015	.35	316
	.178	.059		2400	.016	.35	317
	.178	.059	↓	1700	.013	.35	318
1.25	0.117	1.51	Singly charged helium ions	3700	0.070	0.68	138
	.117	1.51	↓	3000	.063	.68	139
	.117	1.51		3100	.064	.68	140
	.102	.90		4100	.204	.78	165
	.102	.90		4100	.204	.78	166
	.059	.96		3950	.324	.95	217
	.059	.96		4150	.33	.95	218
	.059	.96	↓	4450	.34	.95	219

TABLE V. - Concluded. RAW EXPERIMENTAL DATA

Nondimensional radius, α	Axial distance between B_{min} and B_{max}, z_o, m	Average magnetic field, B_{av}, W/m^2	Charge species	Critical deuteron energy, V, eV	Adiabatic parameter, ϵ	Mirror ratio, R_m	Run
1.25	0.133	0.029	Electrons	3000	0.048	0.56	243
	↓	.029	↓	2900	.047	.56	244
		.029		2800	.047	.56	245
		.038		3400	.040	.52	261
		.038		3300	.039	.52	262
		.038		2600	.034	.52	263
	.146	.053		4200	.030	.43	278
	.146	.053		3700	.028	.43	279
	.146	.053	↓	4400	.031	.43	280
1.50	0.102	0.90	Singly charged helium ions	4200	0.206	0.78	167
	.102	.90	↓	4300	.209	.78	168
	.102	.90		4500	.213	.78	169
	.059	.96		3700	.314	.95	220
	.059	.96		3600	.310	.95	221
	.059	.96	↓	3750	.316	.95	222
1.75	0.102	0.90	Singly charged helium ions	2700	0.165	0.78	170
	.102	.90	↓	3500	.188	.78	171
	.102	.90		3100	.177	.78	172
	.059	.96		4450	.34	.95	223
	.059	.96		4150	.33	.95	224
	.059	.96	↓	4000	.33	.95	227

TABLE VI. - PARAMETERS ϵ_1 AND A_1

FOR BEST FIT TO DATA FROM

PRESENT EXPERIMENT

(a) Experimental data.

Nondimensional radius, α	ϵ_1	A_1	Number of data points
0	0.3473	0.3854	49
.25	.3551	.3731	48
.50	.3580	.3670	35
.75	.3692	.3435	33
1.00	.3725	.3265	23
1.25	.4022	.2916	17
1.50	.3518	.4904	6
1.75	.4036	.3062	6

TABLE VI. - Concluded. PARAMETERS ϵ_o AND A FOR BEST FIT TO DATA FROM PRESENT EXPERIMENT

(b) Transformed experimental data.

Nondimensional radius, α	ϵ_o	A	Number of data points
0	0.3472	0.3858	49
.25	.3524	.3820	48
.50	.3464	.4041	35
.75	.3557	.4120	33
1.00	.3558	.4399	23
1.25	.3839	.4474	17

TABLE VII. - CRITICAL ENERGY AS FUNCTION OF AZIMUTHAL ANGLE FOR REFERENCE DEVICE

Radial mirror ratio, δ	Nondimensional radius, α	Fraction of particles adiabatic, F, percent	Number of pairs of multipolar currents, n	Azimuthal angle, θ	A	ϵ_0	Critical energy, V, eV
0.50	0.50	0.50	2	$-\pi/2$	0.4684	0.1308	8.40×10^5
				$-\pi/4$	.4123	.1236	5.10
				0	.4475	.1032	4.65
				$\pi/4$	.4610	.1108	5.80
				$\pi/2$	.4684	.1308	8.40

TABLE VIII. - DEWAR HEAT-TRANSFER CHARACTERISTICS

Canisters	Time between fills, hr	Boiloff, liter/hr
Stationary Dewar, liquid helium	12.3	0.70 helium
Movable Dewar, liquid helium	10.0	.95 helium
Stationary Dewar, liquid nitrogen	12.7	.67 nitrogen
Movable Dewar, liquid nitrogen	8.8	.70 nitrogen

"The aeronautical and space activities of the United States shall be conducted so as to contribute . . . to the expansion of human knowledge of phenomena in the atmosphere and space. The Administration shall provide for the widest practicable and appropriate dissemination of information concerning its activities and the results thereof."

—NATIONAL AERONAUTICS AND SPACE ACT OF 1958

NASA SCIENTIFIC AND TECHNICAL PUBLICATIONS

TECHNICAL REPORTS: Scientific and technical information considered important, complete, and a lasting contribution to existing knowledge.

TECHNICAL NOTES: Information less broad in scope but nevertheless of importance as a contribution to existing knowledge.

TECHNICAL MEMORANDUMS: Information receiving limited distribution because of preliminary data, security classification, or other reasons.

CONTRACTOR REPORTS: Technical information generated in connection with a NASA contract or grant and released under NASA auspices.

TECHNICAL TRANSLATIONS: Information published in a foreign language considered to merit NASA distribution in English.

TECHNICAL REPRINTS: Information derived from NASA activities and initially published in the form of journal articles.

SPECIAL PUBLICATIONS: Information derived from or of value to NASA activities but not necessarily reporting the results of individual NASA-programmed scientific efforts. Publications include conference proceedings, monographs, data compilations, handbooks, sourcebooks, and special bibliographies.

Details on the availability of these publications may be obtained from:

SCIENTIFIC AND TECHNICAL INFORMATION DIVISION

NATIONAL AERONAUTICS AND SPACE ADMINISTRATION

Washington, D.C. 20546